The Glc7/PP1 phosphatase triggers Paf1C dissociation from RNA polymerase II to enable transcription termination

Sanchirmaa Namjilsuren and Karen M. Arndt*

Department of Biological Sciences, University of Pittsburgh, Pittsburgh, PA 15260, USA

*Correspondence: arndt@pitt.edu

SUMMARY

The mechanisms that control the dynamic composition of RNAPII elongation complexes govern major transitions in the transcription cycle yet are poorly understood. Here, we show that the transcription elongation factor Spt5 determines elongation complex composition to promote productive elongation and the transition to termination. Using an unbiased genetic screen and genomic approaches in *Saccharomyces cerevisiae*, we provide evidence that dephosphorylation of the Spt5 C-terminal repeat domain (CTR) by the Glc7/PP1 phosphatase is required to dislodge Paf1C from RNAPII near the cleavage and polyadenylation site (CPS). Mutations in Paf1C or the Spt5 CTR that dissociate Paf1C from RNAPII bypass the requirement for two critical regulatory subunits of Glc7. Depletion of Glc7 causes aberrant retention of Paf1C past the CPS and increased readthrough transcription, which is fully suppressed by Paf1C mutations. We conclude that Paf1C antagonizes termination and Glc7-mediated restructuring of the RNAPII elongation complex is a critical step in transcription termination.

INTRODUCTION

Many factors associate with RNAPII to coordinate co-transcriptional events that drive major transitions in the transcription cycle. Early in the transition from initiation to elongation, a set of highly conserved transcription elongation factors, including Spt5, Spt6 and Polymerase Associated Factor 1 Complex (Paf1C), assembles onto RNAPII and promotes productive transcription through nucleosomes.[1,2] Many additional factors engage with this core RNAPII elongation complex to couple transcription with RNA processing and chromatin regulation and to facilitate the transition from transcription elongation to termination.[1-4] The dynamic association of these factors with RNAPII is often controlled by protein kinases and phosphatases that target the C-terminal domain (CTD) of the largest subunit of RNAPII, Rpb1, or the elongation factor Spt5.[5,6] For some of these interactions, the temporal controls and structural interfaces have been documented. However, much less is known about the mechanisms that direct changes to the composition of RNAPII elongation complexes across active genes or the consequences when these mechanisms fail.

Spt5, in a heterodimeric complex with Spt4 (DSIF in humans),[7,8] is one of the first elongation factors to associate with RNAPII upon promoter escape, and its occupancy pattern largely mirrors RNAPII post initiation.[9] Spt5 promotes RNAPII processivity, co-transcriptional mRNA processing, and chromatin maintenance, and it regulates RNAPII promoter-proximal pausing in metazoans.[6,10,11] Some of these functions are mediated by the Spt5 C-terminal repeat domain (CTR) and its phosphorylation by CDK9 (Bur1 in *Saccharomyces cerevisiae*).[6,12-15] The CTR is a conserved feature of eukaryotic Spt5, consisting of repeats of a consensus sequence, although the number of repeats and the consensus sequence vary between species.[14-17] In *S. cerevisiae*, the Spt5 CTR contains 15 repeats of S[T/A]WGG[A/Q], in which the first serine residue can be phosphorylated.[12,17] The Spt5 CTR serves as an interaction hub for multiple factors, including Paf1C[12,15,18-21] and pre-mRNA capping[22-26] and cleavage factors.[27]

CTR phosphorylation converts human SPT5 from a negative factor to a positive one, thereby facilitating RNAPII release from promoter-proximal pausing into productive elongation.[6,28-32]

Paf1C, a multi-functional protein complex, is another highly conserved elongation factor associated with RNAPII. In yeast, Paf1C consists of five subunits, Paf1, Ctr9, Cdc73, Rtf1, and Leo1.[30,33-35] In metazoans, the complex contains an additional subunit, Wdr61, and Rtf1 is less tightly associated.[30,36] Paf1C directly stimulates transcription elongation, RNAPII processivity and transcription-coupled histone modifications.[20,37-41] Paf1C also contributes to nucleosome positioning through an interaction with the chromatin remodeler Chd1.[42,43] At least three attachment points within the core elongation complex are critical for Paf1C recruitment to RNAPII. Rtf1 interacts with the phosphorylated Spt5 CTR, and Cdc73 interacts with both the Rpb1 linker region and Spt6.[18,20,21,44-47] Mutating any one of these interactions significantly reduces Paf1C chromatin occupancy, suggesting that these mechanisms function nonredundantly in assembling Paf1C onto RNAPII. Intriguingly, despite its direct interactions with the Spt5 CTR, Spt6, and RNAPII, Paf1C has a unique occupancy pattern on transcribed genes. It joins the elongation complex after Spt5 and Spt6 and dissociates from RNAPII near the cleavage and polyadenylation site (CPS). In contrast, Spt5 and Spt6 remain associated with RNAPII downstream of the CPS in the termination zone.[9,48] What determines the position of Paf1C dissociation and the importance of this step for the transition from elongation to termination are unknown.

At the 3' ends of genes, pre-mRNA cleavage and polyadenylation are coupled to transcription termination. Transcription through the polyadenylation signal slows the rate of RNAPII elongation in parallel with the CTD-mediated recruitment of cleavage and termination factors.[4,49,50] Upon pre-mRNA cleavage, the 5' end of the RNAPII-associated transcript is degraded by the 5'-to-3' exoribonuclease Xrn2 (Rat1 in *S. cerevisiae*), leading to destabilization of the RNAPII elongation complex and transcription termination.[51] Spt5 and the phosphorylation

state of the CTR play critical roles in these processes. Studies in budding yeast, fission yeast, and mammalian cells have shown that the PP1 phosphatase dephosphorylates the Spt5 CTR, as well as the RNAPII CTD, at the 3' ends of genes.[13,48,52-56] Through an unknown mechanism, Spt5 CTR dephosphorylation by PP1 slows the rate of elongation near the CPS, allowing the Xrn2 torpedo to catch up with RNAPII.[13,48,54,57] Consistent with its prominent role in termination,[13,48,54,56] PP1 is a component of the phosphatase/APT (associated with Pta1) module of the cleavage and polyadenylation factor complex (CPF in *S. cerevisiae*; CPSF in humans).[58-60] Additionally, the Spt5 CTR has been implicated in cleavage factor recruitment and pre-mRNA cleavage in budding yeast.[27,61] More recently, Spt5 was shown to interact with and stimulate the activity of Xrn2 to promote termination in fission yeast.[62]

While the importance of an Spt5 CTR phosphorylation-dephosphorylation switch in termination is clear, the impact of this switch on the composition and properties of the RNAPII elongation complex remain poorly understood. Here, we provide evidence that dephosphorylation of the Spt5 CTR by Glc7, the sole PP1 in *S. cerevisiae*, promotes dissociation of Paf1C from the RNAPII elongation complex and this is an essential step in transcription termination. Either acute Spt5 depletion or mutations that prevent CTR phosphorylation causes widespread loss of Paf1C from chromatin, while a phosphomimetic Spt5 CTR mutant aberrantly retains Paf1C past the CPS and exhibits increased transcriptional readthrough. Depletion of Glc7 from the nucleus prevents the timely dissociation of Paf1C, Spt5 and RNAPII from chromatin and greatly impairs transcription termination. Remarkably, the deletion of Paf1C subunits fully suppresses transcriptional readthrough at both protein-coding and snoRNA genes caused by nuclear depletion of Glc7. Moreover, mutations that uncouple Paf1C from RNAPII bypass the requirement for two critical regulatory subunits of Glc7 in the phosphatase/APT module of the CPF. We conclude that the essential function of Glc7 in the

context of CPF is to dislodge Paf1C from RNAPII to enable the elongation-to-termination transition.

RESULTS

Acute depletion of Spt5 broadly impacts RNAPII elongation complex assembly and transcription

To investigate the direct roles of Spt5 in RNAPII transcription, we used an auxin inducible degron[63] (AID) to rapidly deplete Spt5 and measured effects on elongation complex assembly by chromatin immunoprecipitation sequencing (ChIP-seq) and RNA synthesis by 4-thiouracil (4tU) labeling of nascent transcripts (4tU-seq).[64] The AID tag on Spt5 (mAID-Spt5) did not interfere with Spt5 function prior to depletion, as the strains grew normally and did not exhibit an Spt$^-$ phenotype (**Figure S1A**). Upon addition of 5-Ph-IAA,[65] mAID-Spt5 was rapidly degraded with little to no change in the levels of Rpb1 or the elongation factors Spt6 and Paf1C (**Figures 1A, S1B, and S1C**). We used 45 minutes as the depletion time for all genomic experiments.

To study the impact of Spt5 on RNAPII elongation complex composition, we measured Rpb1, Paf1C and Spt6 occupancy upon Spt5 depletion. Our spike-in normalized ChIP-seq results showed that, after depletion of Spt5, RNAPII accumulated at the 5' ends of genes and was reduced across gene bodies, as previously reported (**Figures 1B-D**).[62,66-69] Depletion of Spt5 also led to a dramatic loss of the Paf1C subunits Paf1 and Rtf1 from chromatin (**Figures 1B-D and S1D**). At longer times of depletion, bulk levels of Paf1C-dependent histone modifications, H2BK123ub and H3K4me3, also decreased (**Figure S1B**). Furthermore, we observed a strong reduction in Spt6 occupancy, revealing a role for Spt5 in recruiting or retaining Spt6 within the elongation complex (**Figures 1B-D and S1D**). If Spt6 recruitment is

solely dependent on Spt5, we expect that the Spt6:Spt5 ChIP-seq signals would remain unchanged after Spt5 depletion. However, Spt6 occupancy per unit of Spt5 showed an enrichment at the 5' ends of genes, similar to the RNAPII profile, suggesting that Spt6 is recruited to RNAPII, to some extent, in the absence of Spt5 (**Figure 1E**). Given the importance of Spt6 for Paf1C recruitment/retention,[46,70] the loss of Paf1C occupancy upon Spt5 depletion could reflect the combined effects of removing both Spt5 and Spt6 from chromatin. Since neither Spt6[46] nor Paf1C[38] depletion individually causes marked RNAPII accumulation at the 5' ends of genes, this effect of Spt5 depletion can be attributed to a direct function of Spt5 or an unknown interacting partner.

The effect of Spt5 depletion on transcription, assayed by spike-in normalized 4tU-seq, revealed several changes. First, there was a drastic decrease in sense RNA synthesis as well as an increase in antisense transcription concentrated at the 5' ends of genes consistent with previous literature (**Figures 1C, 1F, and 1G**).[66,69] Calculation of the elongation index as a proxy for elongation rate by dividing the 4tU-seq signal by RNAPII ChIP-seq signal[71] showed a severe elongation defect across entire gene bodies (**Figure 1H**). Second, our 4tU-seq data also revealed a widespread splicing defect upon acute loss of Spt5 (**Figures 1I and S1E**), potentially due to a reduced elongation rate.[72] Intron retention was previously observed at both genomic and individual gene levels in Paf1C mutants,[38] upon Spt5 depletion,[69,73] and in a recruitment-defective *spt6* mutant.[74] Considering the crucial role of Spt5 in RNAPII elongation complex assembly as evidenced by our ChIP-seq results, the profound transcriptional defects caused by Spt5 depletion likely arise from the loss of direct Spt5 functions compounded by the effects of also losing Spt6 and Paf1C functions.

The Spt5 CTR is critical for genome-wide occupancy of Paf1C and proper transcription elongation

To investigate the role of the Spt5 CTR in the recruitment defects we observed upon depletion of Spt5, we performed ChIP-seq analysis on a panel of *spt5* CTR mutants. The *spt5* mutations either delete the CTR (*spt5ΔCTR* and *spt5Δ5*) or alter the site of phosphorylation, replacing the first serine residue in all 15 repeats with alanine (*spt5-S1-15A*) or, as a phosphomimetic, aspartic acid (*spt5-S1-15D*) (**Figure 2A**). The *spt5Δ5* mutation, included as a more severe mutation in our genetic screens (below), removes part of the KOW5 domain in addition to the CTR and adjacent linker. To different extents, the ChIP levels of Spt5 were reduced in the mutants, which for three of them can be at least partially explained by decreased protein levels (**Figures 2B, 2C, and S2A**). For the two CTR truncation mutants, the ChIP level of RNAPII is elevated, which further exaggerates the relative level of mutant Spt5 on chromatin (**Figures 2C, S2B, and S2C**). Since there is little effect on RNAPII occupancy levels in the *spt5-S1-15A* or *spt5-S1-15D* mutants, this suggests a phosphorylation-independent function of the CTR in RNAPII transcription.

With respect to other elongation factors, the most dramatic effects of the *spt5* mutations are on Paf1C occupancy. All non-phosphorylatable *spt5* mutants, including *spt5-S1-15A*, *spt5Δ5* and *spt5ΔCTR*, have greatly reduced levels of Paf1 and Rtf1 on chromatin, even when the data are normalized to account for mutant-specific differences in RNAPII and Spt5 occupancy (**Figures 2C and S2B-D**). In contrast, the phosphomimetic *spt5-S1-15D* mutant maintains an intermediate level of Paf1 and Rtf1 occupancy on gene bodies and higher levels of Paf1C association per unit of chromatin-bound Spt5 (**Figures 2C, S2C, and S2D**). These results strongly support a widespread role for Spt5 CTR phosphorylation in Paf1C recruitment to RNAPII, consistent with previous structural studies.[20,21] In contrast to Paf1C, Spt6 occupancy levels largely mirror RNAPII occupancy in all the mutants (**Figures 2C, S2B, and S2C**),

suggesting that Spt6 occupancy depends primarily on the Spt5 core. Interestingly, all non-phosphorylatable *spt5* mutants exhibit an upstream shift of the peaks of RNAPII, Spt5, and Spt6 ChIP-seq signals near the CPS, suggesting changes in RNAPII elongation properties in this region and potential effects on termination (**Figures 2C, S2C, S2E, and S2F**).

Spike-in normalized 4tU-seq analysis of the *spt5* CTR mutants showed distinct effects on transcription. While the truncation and non-phosphorylatable mutants were broadly similar to WT with respect to global 4tU-seq signal levels across gene bodies, the *spt5-S1-15D* mutant exhibited considerably higher transcription (**Figures 2D and 2E**). Elongation index calculations revealed elongation rate defects only in the truncation mutants, indicating that the CTR itself rather than its phosphorylation is crucial for maintaining normal RNAPII activity (**Figure 2F**). The higher elongation index for the *spt5-S1-15D* mutant indicates a greater frequency of RNAPII passage through the gene. To quantify the impact of CTR perturbations on RNAPII processivity, we calculated a completion score as the ratio of 4tU-seq signals within 200 bp windows upstream of the CPS and downstream of the TSS.[38,75] With the notable exception of *spt5-S1-15D*, the *spt5* CTR mutations all cause severe RNAPII processivity defects as indicated by decreasing completion score with increasing gene length (**Figure 2G**). This phenotype correlates with loss of Paf1C from the elongation complex, as either deletion or depletion of Paf1C subunits causes significant RNAPII processivity defects.[38,41] Additionally, all the mutants exhibit increased levels of unspliced transcripts (**Figure 2H**). Given the roles of the Spt5 CTR in pre-mRNA cleavage and RNAPII termination,[13,27,48,61] we quantified transcriptional readthrough as the ratio of 4tU-seq read density within 150 bp windows immediately after and before the CPS.[75] All *spt5* mutants exhibit readthrough transcription to varying degrees (**Figures 2I and S2G**). Notably, the *spt5-S1-15D* mutant shows the most severe termination defect, accompanied by increased Paf1C retention (**Figures S2G and S2H**). Together, our analysis of Spt5 acute depletion and *spt5 CTR* mutants underscores the role of Spt5 as a nexus of RNAPII

elongation complex assembly to promote elongation, transcript processing, and the transition to termination.

Transposition-based mutational screens identify genes that functionally interact with the Spt5 CTR

To interrogate the functions of the Spt5 CTR and its phosphorylation through the identification of genetic interactors, we performed a high-throughput, transposon-based yeast genetic screen, SAturated Transposon Analysis in Yeast (SATAY).[76,77] Since most transposon insertions create a loss-of-function allele, the differences in transposon coverage in a mutant background compared to a wild-type background identify potential genetic interactions. Higher transposon coverage in a given gene in the mutant background relative to the wild-type background indicates suppression while lower coverage indicates synthetic growth impairment or lethality. We performed SATAY screens on *spt5Δ5*, *spt5-S1-15A*, and *spt5ΔCTR* strains. The transposon maps and principal component analysis show high reproducibility between replicates (**Figures 3A and S3A**).

Focusing first on candidates from the screen with the *spt5Δ5* mutant, which appears especially sensitive to genetic changes, the SATAY results revealed many genes with significant enrichment in transcription- and chromatin-associated gene ontology (GO) terms (**Figures 3B and 3C**). We generated deletion mutations *de novo* for 14 genes (**Figure S3B**) to independently test their genetic interactions with the *spt5Δ5* mutation. To this end, we performed growth assays on progeny after yeast tetrad dissection and also tested for effects on the Spt$^-$ phenotype of *spt5Δ5* (**Figures S3C and S3D**). We also calculated fitness and deviation scores to evaluate the genetic interactions (**Figure 3D**).[78] For many of these genes, independent testing either by dilution spot assays or quantitation of colony size after tetrad

dissection verified the SATAY predictions. In some cases, the candidate mutation or *spt5Δ5* was epistatic to the other mutation (**Figure 3D and S3D**).

After these initial tests, we focused on candidates related to two events coupled to transcription elongation: pre-mRNA splicing and transcription termination. Deletion of *MSL1*, which encodes the U2B component of the U2 snRNP,[79] caused a synthetic growth defect with *spt5Δ5* and suppressed the Spt$^-$ phenotype of the *spt5Δ5* mutant (**Figure S3D**). Given the splicing defects observed for *spt5 CTR* and Paf1C mutants (**Figure 2H**),[38] we generated double mutants of *msl1Δ* with a set of *SPT* gene and Paf1C mutations (**Figures S3E-G**). We found that *msl1Δ* was synthetically lethal with *rtf1Δ* and *paf1Δ* mutations, as well as the *spt5-242* mutation, which genetically interacts with multiple factors implicated in elongation control (**Figures S3E and S3F**).[35,80-82] In addition, *msl1Δ* caused synthetic growth defects in combination with *spt5-S1-15A* and *spt6-50* (lacking tSH2 domain) mutations, which dissociate Paf1C from RNAPII (**Figure 2C**).[46] Regarding suppression of the Spt$^-$ phenotype, growth spot assays showed that *msl1Δ* suppressed, to varying degrees, the Spt$^-$ phenotypes of all tested *spt5* mutants as well as *spt6* mutants (**Figure S3G**). Finally, to test the specificity of the interaction with respect to the U2 snRNP, we generated deletions of nonessential genes representing other snRNPs and found that only mutations affecting U2 snRNP components, *msl1Δ* and *lea1Δ*, and the branchpoint binding factor, *mud2Δ*, suppressed the Spt$^-$ phenotype of the *spt5ΔCTR* mutant without major synthetic growth effect (**Figures S3H and S3I**). Although the mechanism of suppression of the Spt$^-$ phenotype is unclear, these results strengthen the functional connections between core elongation factors and pre-mRNA splicing components and suggest a particularly specific connection with the U2 snRNP.

Strikingly, our SATAY screen uncovered strong positive genetic interactions between *spt5* CTR mutations and mutations targeting the CPF, specifically its phosphatase/APT module. Compared to wild type, we observed a significantly higher number of transposon insertions in

the *REF2* gene in the *spt5Δ5* background (**Figures 3D and S4A**) and in the *SWD2* gene in all three *spt5* CTR mutant backgrounds (**Figures 3B, 3E-G, and 4A**). *REF2* and *SWD2* encode critical regulatory subunits of Glc7 in the phosphatase/APT module.[58-60,83-85] The increased transposition in *REF2* and *SWD2* indicates that the *spt5* CTR mutations suppress the severe growth defects and inviability normally associated with the loss of Ref2 or Swd2, respectively.[83,85] Consequently, the increased fitness of *ref2 spt5* and *swd2 spt5* double mutants, compared to the single mutants, leads to their higher representation in the pools of cells that have undergone transposition. Overall, the identification of two components of the Swd2-Ref2-Glc7 submodule in our genetic screen points to a specific functional interaction between the Spt5 CTR and the phosphatase/APT module of the CPF.

Disruption of Paf1C recruitment to RNAPII suppresses loss of Swd2 and Ref2

Building on the SATAY results, we further investigated the genetic suppression of *ref2* and *swd2* mutations by *spt5* CTR mutations. First, we generated *swd2*Δ and *ref2*Δ alleles *de novo* and confirmed their lethality/extreme growth defects in our genetic background, which is consistent with the dearth of transposon coverage within these genes (**Figures 4A, S4A, and S4B**). Next, we generated double mutants of *swd2*Δ or *ref2*Δ with the *spt5* mutations to confirm and extend the genetic interaction results (**Figures 4B and 4C**). All non-phosphorylatable *spt5* CTR mutations rescued the lethality/extreme growth defects of the *swd2*Δ and *ref2*Δ mutants, suggesting that Spt5 CTR phosphorylation is toxic to cells in the absence of Swd2 or Ref2. The phosphomimetic *spt5-S1-15D* mutant rescues the growth defect of the *ref2*Δ mutant, albeit to a partial extent, but not *swd2*Δ lethality. Our ChIP-seq results showed that Paf1C occupancy is severely reduced in the non-phosphorylatable *spt5 CTR* mutants, whereas the *spt5-S1-15D* mutant has an intermediate level of Paf1C occupancy (**Figure 2C**). Therefore, we tested whether Paf1C mutations could also rescue the lethality/extreme growth defects of *swd2*Δ and

*ref2*Δ mutants. Indeed, both *paf1*Δ and *rtf1*Δ strongly suppressed the *ref2*Δ and *swd2*Δ mutations (**Figure 4D**). Given the less severe nature of *ref2*Δ compared to *swd2*Δ, the partial reduction in Paf1C occupancy in the *spt5-S1-15D* mutant might be sufficient to suppress *ref2*Δ but not *swd2*Δ.

Since Paf1C is a multifunctional complex,[86] we asked which specific function of Paf1C, when defective, overcomes the lethal consequences of deleting *SWD2*. To this end, we tested *rtf1* separation-of-function mutations for their ability to rescue *swd2*Δ lethality. These *rtf1* mutations disrupt its interaction with the chromatin remodeler Chd1 (*rtf1-8-9A*),[42,43] ability to stimulate histone H2BK123ub (*rtf1-108-110A*),[37,40] or interaction with the Spt5 CTR for recruitment (*rtf1*Δ*7*).[87] The first two mutations did not have any effect on *swd2*Δ lethality, whereas strong suppression was observed with the *rtf1*Δ*7* mutation, which removes a portion of the Spt5 CTR-interacting Plus3 domain of Rtf1 (**Figures 4E and S4C**).[18,21,87] Suppression of *swd2*Δ lethality was also observed for the Paf1C recruitment-defective *cdc73*Δ*C* mutation, which removes the domain in Cdc73 that interacts with Spt6 and the Rpb1 linker (**Figure 4E**).[44-46] Consistent with the tetrad dissection results, conditional expression of *RTF1* from a galactose-inducible plasmid restored *swd2*Δ and *ref2*Δ *swd2*Δ lethality (**Figure 4F**). Even low levels of leaky *RTF1* expression from this plasmid in glucose conditions impaired growth in the context of *swd2*Δ and *ref2*Δ mutations. Collectively, these results strongly suggest that, in the absence of a functional Swd2-Ref2-Glc7 submodule, the association of Paf1C with RNAPII is lethal.

Swd2 and Ref2 are required for Glc7 occupancy at the 3' ends of genes

Biochemical evidence shows that loss or mutation of Ref2 or Swd2 leads to dissociation of Glc7 from the CPF.[59,60,88] Therefore, we hypothesized that Glc7 would fail to associate with chromatin in the absence of Ref2 and Swd2, particularly at the 3' ends of genes. To test this hypothesis, we took advantage of the viable *rtf1*Δ *ref2*Δ *swd2*Δ triple mutant to profile Glc7,

RNAPII, and Spt5 occupancies by ChIP-seq. Western blot analysis showed comparable bulk levels of RNAPII, Spt5, and HA-Glc7 in the triple mutant and the *rtf1*Δ control strain (**Figure 5A**). In agreement with Swd2 also being a member of the Set1 histone methyltransferase complex,[83,89] H3K4me1 was undetectable in the triple mutant compared to a highly reduced level in the *rtf1*Δ strain. The Glc7/PP1 submodule is normally enriched at the 3' ends of genes with peak occupancy just downstream of the CPS (**Figures 5B and 5C**).[48] However, Glc7 was greatly depleted from the 3' ends of genes in the triple mutant, supporting a requirement for Swd2 and Ref2 in tethering Glc7 to the CPF *in vivo* (**Figures 5B-D**). Chromatin occupancy of RNAPII (Rpb3 and Rpb1 subunits) and Spt5 was elevated in an *rtf1*Δ-dependent manner, potentially due to slower RNAPII elongation (**Figures 5B, 5C, and S5A**). Interestingly, Spt5 signal per unit of RNAPII drops off earlier near the CPS in the *rtf1*Δ mutants, suggesting that Spt5 may become prone to dissociation in the absence of Paf1C (**Figure S5B**).

To assess the consequences of Glc7 dissociation from the CPF on transcript synthesis, we performed 4tU-seq on the same set of mutants. Spike-in normalized 4tU-seq analysis revealed a global increase in both sense and antisense transcription in the triple mutant relative to the *rtf1*Δ single mutant (**Figures 5C, 5E, and S5C**). The elongation index pointed to increased RNAPII passage through gene bodies in the triple mutant (**Figures S5D and S5E**). Importantly, the triple mutant also showed increased transcriptional readthrough, particularly for the most highly transcribed genes (**Figures 5F and 5G**). Defects in splicing and RNAPII processivity were also observed for the triple mutant, expanding the roles of the Swd2-Ref2-Glc7 phosphatase submodule beyond pre-mRNA cleavage and termination (**Figures S5F and S5G**). Collectively, our results show that Swd2 and Ref2 are required for the localization of Glc7 at the 3' ends of genes, efficient transcription termination and suppression of aberrant transcriptional activity within gene bodies. They also show that dissociation of Paf1C from RNAPII overcomes the requirement for Glc7 at the 3' ends of genes.

Glc7 is required to trigger dissociation of Paf1C from RNAPII at the CPS

Since the Swd2-Ref2-Glc7 phosphatase submodule becomes dispensable for viability in the absence of Paf1C, we hypothesized that the essential function of Glc7 in the CPF is to dislodge Paf1C from RNAPII to facilitate the elongation-to-termination transition. To test this hypothesis, we conditionally depleted Glc7 from the nucleus using the anchor-away system.[90] Coupled with ChIP-seq, we profiled RNAPII, Spt5 and Paf1C occupancies. Based on a time course (**Figure S6A**) and the literature,[56] we treated experimental (*GLC7-3xHA-FRB*) and control (*GLC7-3xHA*) strains with rapamycin for one hour to induce nuclear depletion of FRB-tagged Glc7.

Western analysis after Glc7 nuclear depletion showed no adverse effects on total protein abundance of RNAPII and elongation factors (**Figure 6A**). Spt5 CTR phosphorylation increased after depletion as measured by an antibody against the phosphorylated CTR.[12] For the *GLC7-3xHA-FRB* strain, this result is consistent with work in *S. pombe* and human cells showing PP1-dependent dephosphorylation of Spt5.[13,48,54] However, for reasons unknown, we also observed a moderate elevation in Spt5 CTR phosphorylation for the *GLC7-3xHA* control strain. We therefore included this rapamycin-treated control strain in all our ChIP-seq experiments. Spt5 hyperphosphorylation was also observed in the *glc7-T152K* mutant,[91] further supporting Glc7 as the evolutionarily conserved Spt5 CTR phosphatase in *S. cerevisiae* (**Figure S6B**).

For the *GLC7-3xHA-FRB* strain, Glc7 chromatin occupancy was greatly reduced after one hour of rapamycin treatment (**Figures 6B-D, S6C, and S6D**). Strikingly, the occupancy levels of RNAPII, Spt5 and Rtf1 downstream of the CPS were all elevated upon nuclear depletion of Glc7 (**Figures 6B-D, S6C, and S6D**). This 3' retention of RNAPII was expected based on previous reports of PP1-dependent termination in mammalian cells,[48] *S. pombe*,[13,54] and *S. cerevisiae*.[56,60] Our findings reveal that, when normalized to RNAPII and Spt5 ChIP-seq signals, Paf1C exhibits the highest increase in chromatin occupancy downstream of the CPS

upon Glc7 depletion (**Figures S6E and S6F**). Importantly, the control strain (*GLC7-3xHA*) for rapamycin treatment and the vehicle-treated (DMSO) Glc7 anchor-away strain showed similar occupancy profiles, confirming that the observed effects are due to nuclear depletion of Glc7 (**Figure 6B**). Overall, the ChIP-seq results strongly suggest that Glc7 function in the CPF is required for the dissociation of Paf1C, Spt5, and RNAPII during the elongation-to-termination transition.

Paf1C antagonizes transcription termination in the absence of Glc7

Hypothesizing that depletion of Glc7 from the nucleus would phenocopy the effects of *swd2*Δ and *ref2*Δ mutations in the context of CPF, we asked if *rtf1*Δ and *paf1*Δ mutations could suppress the effects of Glc7 nuclear depletion at the level of transcription as measured by 4tU-seq. Notably, neither *rtf1*Δ nor *paf1*Δ was able to rescue the lethality caused by nuclear depletion of Glc7, suggesting that Glc7 likely has other essential, CPF-independent functions in the nucleus (**Figure S7A**). Western blot analysis showed no rapamycin-dependent changes in Ser2P and Ser5P levels, even in the *paf1*Δ strain with highly reduced Ser2P levels,[92] in agreement with previous studies on PP1 (**Figure S7B**).[54,56] Meanwhile, in each strain, the Spt5 phosphorylation signal consistently increased upon nuclear depletion of Glc7 (**Figure S7B**).

Depletion of Glc7 from the nucleus increased both sense and antisense transcription across gene bodies in the wild-type background (**Figures 7A and S7C**). In contrast, a global reduction or no change in 4tU-seq signal was observed in the *paf1*Δ and *rtf1*Δ mutants. Consistent with previous studies[56] and RNAPII retention by ChIP-seq, we observed widespread transcriptional readthrough upon nuclear depletion of Glc7 (**Figures 7B-D, S7D, and S7E**). The severity of readthrough was positively correlated with gene expression level (**Figure 7D**). Remarkably, the transcription termination defects brought on by Glc7 anchor-away were almost entirely suppressed by the *paf1*Δ and *rtf1*Δ mutations (**Figures 7B-D, S7D, and S7E**). Given the

requirement for Glc7 in snoRNA termination,[59,60,84] we also looked at snoRNA gene transcription and found extreme 3' readthrough upon Glc7 anchor-away, which was fully corrected by *paf1*Δ or *rtf1*Δ mutation (**Figures S7F and S7G**).

Together, our results demonstrate that inappropriate retention of Paf1C antagonizes transcription termination. As Paf1C is a positive regulator of transcription elongation,[20,38,39,41,93] it is possible that slower RNAPII elongation rates in Paf1C mutants allow extra time for the Glc7-deficient CPF to function and alleviate the transcriptional readthrough defect. In support of this idea, the *rpb1-E1103G* and *rpb1-H1085Q* mutations, which slow elongation *in vivo*,[94] also rescued *swd2*Δ lethality (**Figure 7E**). These results are consistent with a kinetic competition model between transcription-coupled processes governed by Paf1C; however, mechanisms related to the dynamics of transcription factor exchange may also contribute to the anti-termination effects of Paf1C retention.

DISCUSSION

In this study, we investigated the mechanisms that control the composition of RNAPII elongation complexes and their impact on the transition from transcription elongation to termination. Through yeast genetics and quantitative genomic approaches, we demonstrate that Spt5 CTR phosphorylation controls Paf1C residence in the RNAPII elongation complex. This, in turn, determines whether localization of the Glc7 phosphatase at the 3' end of genes is strictly required for transcription termination. Mutations detaching Paf1C from RNAPII bypass the requirement for a functional Glc7 module in the CPF, and conditions leading to inappropriate retention of Paf1C past its normal site of dissociation near the CPS antagonize termination. We conclude that transcription termination requires dissociation of the positive elongation factor Paf1C from RNAPII through Glc7-mediated dephosphorylation of the Spt5 CTR.

To provide a benchmark for our studies on Spt5 CTR mutants, we first investigated the direct functions of Spt5 using an acute depletion strategy. Our results demonstrated a widespread requirement for Spt5 in the assembly of competent RNAPII elongation complexes and transcript synthesis, consistent with previous depletion studies.[62,66,67,69] While global occupancy of Spt5 is not affected by Spt6 depletion,[46] our studies uncovered a genome-wide dependence of Spt6 chromatin association on Spt5. Specifically, we found that upon Spt5 depletion, Spt6 occupancy is strongly reduced on gene bodies presumably due to the loss of its binding surfaces on Spt5 and the Rpb4/7 stalk in RNAPII.[20,30,45,95] Interestingly, Spt6 can still associate with RNAPII to some extent at the 5' ends of genes when Spt5 is depleted, potentially through an interaction with the RNAPII linker.[96] Therefore, the increased antisense transcription detected upon Spt5 depletion likely arises from the combined loss of direct Spt5 functions, such as its histone binding activity,[10,97] and the histone chaperone activity of Spt6.[98]

Our comparative analysis of *spt5* mutations revealed multi-layered regulation of gene expression by the Spt5 CTR and its phosphorylation, including effects on Paf1C occupancy and RNAPII processivity as well as splicing and termination efficiency. For the *spt5ΔCTR* mutant, our observations are consistent with previous findings linking the CTR to termination efficiency.[27,61] With respect to the substitution mutants, the phosphomimetic *spt5-S1-15D* mutant exhibited more severe transcriptional readthrough than the *spt5-S1-15A* mutant. Based on our SATAY screens and follow-up studies, we propose that this difference in readthrough propensity largely reflects a difference in Paf1C recruitment/retention in these mutants. The *spt5-S1-15D* mutant exhibited intermediate levels of Paf1C on gene bodies and Paf1C retention past the CPS, whereas the *spt5-S1-15A* mutant was nearly devoid of chromatin-associated Paf1C. Indeed, several genetic interactors identified in our SATAY screens with *spt5* CTR mutants also genetically interact with Paf1C mutations, highlighting the close functional relationship between Spt5 CTR phosphorylation and Paf1C. Similarly, among all mutants tested,

the *spt5-S1-15D* mutant was uniquely unaffected for RNAPII processivity, suggesting that the Spt5 CTR promotes RNAPII processivity, possibly in large part, through phosphorylation-mediated Paf1C recruitment.[38,39,41] However, since the *spt5 CTR* truncation mutants exhibited more severe elongation and mRNA processing defects than the nonphosphorylatable *spt5-S1-15A* mutant despite similar reductions in Spt5 and Paf1C occupancies, our data also support Paf1C-independent functions of the CTR in transcription.

Prompted by our SATAY results, we showed that mutations impairing the U2 snRNP are synthetically lethal with *spt5-242* and Paf1C mutations and suppress the Spt$^-$ phenotypes of several *spt5* and *spt6* mutants. Mutations in *RPB1* that slow catalysis by RNAPII are also synthetically lethal with Paf1C mutations[99,100] and suppress the Spt$^-$ phenotypes of *spt5-194, spt5-242* and *spt4*Δ mutants.[80] These results suggest that the U2 snRNP may possess an elongation-promoting function. In mammalian cells, both U1 and U2 snRNPs are positive regulators of transcription,[71,101] and the interplay between elongation rates and co-transcriptional splicing is an area of active research.[102] The spliceosome also regulates chromatin structure through direct and indirect mechanisms,[103,104] and the combined effects on chromatin of losing both spliceosomes and elongation factors, which themselves impact chromatin states, may be below the threshold for cell viability. Indeed, synthetic lethal interactions between the absence of the Paf1C-dependent histone mark H2BK123ub and deletions of two U2snRNP genes, *MSL1* and *LEA1,* have been reported.[105]

The most striking result from our SATAY screen and subsequent genetic experiments was the strong suppression of *swd2* and *ref2* mutations by the absence of Spt5 CTR phosphorylation or by mutations disrupting Paf1C recruitment to RNAPII. Mutations that disrupt the interface between Ref2 and Glc7 are lethal due to the loss of Glc7 from the CPF, emphasizing the essential function of Glc7 in the CPF.[60,88] Capitalizing on the viable *rtf1*Δ *ref2*Δ *swd2*Δ triple mutant, we confirmed that Swd2 and Ref2 are required for the localization of Glc7

to the 3' ends of genes *in vivo*. The fact that the Swd2-Ref2-Glc7 submodule of the CPF is dispensable in the absence of Paf1C argues that the essential function of this submodule is to dislodge Paf1C from RNAPII. Indeed, nuclear depletion of Glc7 caused retention of Paf1C beyond its normal dissociation site near the CPS and widespread termination defects that were nearly fully reversed by deletion of Paf1C subunits. Previous reports in mammalian cells,[48,106] fission yeast[13,54] and budding yeast[56] showed that the deletion or depletion of PP1/Dis2/Glc7 phosphatase causes an RNAPII termination defect. In addition, Glc7 phosphatase activity in the APT complex is critical for snoRNA termination.[59,60,84] We showed that nuclear depletion of Glc7 caused Paf1C retention and severe readthrough transcription of snoRNA genes, which was also strongly suppressed by Paf1C mutations. This is in contrast with reports that Paf1C and its dependent histone modifications are required for efficient snoRNA 3'-end formation.[107-111] In those earlier studies, steady state snoRNA transcript levels were measured whereas we used nascent transcriptomics, suggesting that deletion of Paf1C might stabilize snoRNA readthrough transcripts. Because we also see a global increase in transcriptional output in the *rtf1*Δ *ref2*Δ *swd2*Δ triple mutant and upon nuclear depletion of Glc7, the Swd2-Ref2-Glc7 submodule may also function as a negative regulator of transcription elongation. Considering that Paf1C mutations suppress this global increase in transcription when Glc7 is sequestered from the nucleus, Glc7 may negatively regulate transcription by limiting the levels of Paf1C associated with RNAPII on gene bodies.

In combination, our data strongly suggest that aberrant Paf1C retention on RNAPII through Spt5 CTR hyperphosphorylation underlies the termination defects caused by loss of the Glc7 phosphatase submodule of the CPF. This would also explain elevated 3' readthrough in the phosphomimetic *spt5-S1-15D* mutant. We note, however, that the *spt5-S1-15D* mutant does not fully phenocopy nuclear depletion of Glc7 at the level of transcription, possibly due to globally reduced Spt5 occupancy and/or multiple targets of Glc7 in the RNAPII complex

including the RNAPII CTD. It is also notable that transcriptional readthrough caused by nuclear depletion of Glc7 was almost entirely suppressed by *rtf1*Δ and *paf1*Δ, whereas a moderate level of 3' readthrough was evident in the *rtf1*Δ *ref2*Δ *swd2*Δ triple mutant albeit less than that observed in the Glc7 anchor-away condition in the presence of *RTF1* and *PAF1* (**Figure S7D-G**). This discrepancy could arise from at least two sources. The triple mutant likely represents an equilibrated state of the viable, suppressed condition and might have less 3' readthrough than the *ref2*Δ *swd2*Δ double mutant, which is inviable. Alternatively, Ref2 and Swd2 might have Glc7-independent functions in the CPF. For example, Ref2 is critical for the interaction between APT and RNAPII biochemically[88] and the recruitment of the rest of the CPF complex may be compromised in the triple mutant.

Two non-mutually exclusive mechanisms could explain how Paf1C antagonizes mRNA cleavage and transcription termination. (1) RNAPII fails to decelerate past the CPS due to the elongation-promoting activity of Paf1C. In fact, Spt5 dephosphorylation by PP1 in mammalian cells is critical for RNAPII deceleration[13,48] and downstream poly(A) sites are favored by fast RNAPII mutants.[112] Moreover, depletion of Paf1C subunits in mammalian cells leads to a 5'-shift in poly(A) site selection.[113] (2) Paf1C physically occludes the binding surface on RNAPII for cleavage and termination factors. There is evidence of a direct interaction between RNAPII and CPF[88] and Xrn2.[51,62] Although we provide genetic evidence in support of the kinetic competition mechanism, further structural and biochemical studies are needed to test the second mechanism. A recent study reported a direct interaction between the Glc7 phosphatase submodule and the RNAPII core, and subsequent CTD dephosphorylation-mediated RNAPII dimerization.[88] This could reflect an RNAPII state after dissociation of elongation factors during termination, and it will be interesting to learn how Spt5 and its dephosphorylation affect these interactions.

Finally, in the context of current literature, we propose a model (**Figure 7F**) wherein the CPF is recruited by its interaction with Ser2P of the RNAPII CTD[114-116] at the 3' ends of genes and triggers dissociation of Paf1C through dephosphorylation of the Spt5 CTR[13,48,54] and likely additional targets such as Tyr1P of the RNAPII CTD.[53,56,117] Removal of Paf1C slows RNAPII elongation and enables CPF access to RNA and/or RNAPII for efficient pre-mRNA cleavage and transcription termination. Paf1C has been reported to interact with the Cft1 subunit of the CPF[92] and therefore may play a role in recruiting CPF prior to its dissociation. In summary, we have uncovered the molecular basis of termination defects observed upon Glc7 depletion and a previously underappreciated role of Paf1C in antagonizing termination.

ACKNOWLEDGEMENTS

We are thankful to Grant Hartzog, Alan Hinnebusch, Fred Winston, Steven Hahn, Tim Formosa, Kevin Struhl, Craig Kaplan, Nathan Clark and John Woolford for providing yeast strains, antibodies, or plasmids. We thank Benoit Kornmann for sharing the SATAY plasmid and a data analysis script with us. We thank Margaret Shirra for generating integrated *spt5* substitution mutants and Tasniem Fetian for the *Os*TIR1-F74G strain used for a genetic cross. We also acknowledge previous members of the lab, Mitchell Ellison, Sonia Fung, and Lydia Caldwell for their contributions in early stages of the research. We are grateful to Sarah Hainer and Weifeng Xu for sharing equipment. We thank Sarah Hainer, Craig Kaplan, Miler Lee, Carl Wu, members of their groups, and all members of the Arndt lab for helpful discussions. This project used the University of Pittsburgh Health Sciences Sequencing Core at UPMC Children's Hospital of Pittsburgh for NGS experiments and was supported in part by the University of Pittsburgh Center for Research Computing through the resources provided. This work was supported by an Andrew Mellon Predoctoral fellowship to S.N. and NIH grant R35 GM141964 to K.M.A.

Figure 1. Spt5 is required for RNAPII elongation complex assembly and productive transcription.

(A) Western blot analysis of mAID-Spt5 depletion. Controls include a strain lacking the mAID tag on Spt5 (WT), cells treated with vehicle (DMSO), and cells collected before addition of 5-Ph-IAA or DMSO (Pre). G6PDH serves as a loading control. Short and long exposures are shown. n=3

(B) Metaplots of mean spike-in normalized ChIP-seq signal for the indicated proteins over non-overlapping *S. cerevisiae* genes (n=3,057)[118] scaled from transcriptional start sites (TSS) to cleavage and polyadenylation sites (CPS). Shading highlights the region between the annotated TSS and CPS. *mAID-SPT5* cells were treated with 5-Ph-IAA (red) or DMSO (black) for 45 min. Color scheme is the same throughout the figure. n=2

(C) ChIP-seq and 4tU-seq sense-strand signal at a highly transcribed locus.

(D) Heatmaps of $\log_2$-fold change in ChIP-seq signal for depleted (5-Ph-IAA) vs. undepleted (DMSO) conditions as in (B) with genes sorted by length. Dashed line indicates CPS.

(E) Heatmap of Spt6 ChIP-seq signal relative to Spt5 signal.

(F and G) Metaplot (F) and differential heatmap (G) of mean spike-in normalized 4tU-seq signal for sense and antisense transcripts for genes shown in (B). n=2

(H) Metaplot of elongation index.

(I) Boxplot of splicing efficiency at the 5' splice junction of introns (n = 231) per Tukey method. Significance from Mann-Whitney U test with FDR correction: ***$p < 0.001$.

Figure 2. The Spt5 CTR and its phosphorylation regulate multiple aspects of RNAPII transcription.

(A) Spt5 mutants used for ChIP-seq and 4tU-seq experiments. Color code is used throughout the figure. Diagram at the top illustrates the domain structure of *S. cerevisiae* Spt5 with domains/regions labeled as NGN=NusG N-terminal homology, I=insertion, and K=KOW.[119]

(B) Western blot analysis of *spt5* mutant strains. Black bar indicates the same strains/replicates. n=3

(C and D) Metaplots of mean spike-in normalized ChIP-seq signal for the indicated proteins (C) and 4tU-seq signal for the sense-strand (D) over non-overlapping genes. n=2

(E) Heatmap representation of $\log_2$-fold change in 4tU-seq sense-strand signal for *spt5* mutants relative to WT.

(F) Metaplot of elongation index.

(G-I) Boxplots report the $\log_2$-fold change in completion score stratified by gene-length class (G) distribution of splicing efficiency over the 5' splice junction of introns (n = 231) (H), and readthrough index (I) as calculated from 4tU-seq data with outliers shown per Tukey method. Black line in (I) indicates median readthrough index of WT. Significance from Mann-Whitney U test with FDR correction: *$p < 0.05$, **$p < 0.01$, and ***$p < 0.001$.

Figure 3. Transposon mutagenesis screens identify genetic interactions with *spt5* CTR mutations.

(A) UCSC genome browser tracks showing transposon coverage at *SPT5* and neighboring genes in strains expressing WT or mutant derivatives of Spt5. Rep numbers indicate independent biological replicates. For some biological replicates, multiple technical replicates were tested.

(B and E-F) Volcano plots showing genes with significantly different numbers of transposon insertions in *spt5Δ5* (B), *spt5ΔCTR* (E) or *spt5-S1-15A* (F) mutants compared to WT as defined by DESeq2. p.adj < 0.05 and $\log_2FC > 1$ or $\log_2FC < -1$. To account for differences in transposition efficiency, the number of transposons per gene (tn/gene) was normalized to the total number of transposons in each replicate.

(C) Bar graph showing top ten overrepresented Gene Ontology (GO)[120] terms associated with total genes with significantly different tn/gene in the *spt5Δ5* mutant.

(D) Bar graph showing deviation score for double mutants of candidate gene deletions with *spt5Δ5*. Fitness was calculated from quantified colony size (in pixels) on yeast tetrad dissection plates. A positive deviation score indicates genetic suppression or epistatic genetic interaction, while a negative deviation score indicates a synthetic impaired growth defect.

(G) Venn diagrams showing the overlaps between genes with significantly greater (up) or fewer (down) tn/gene in the *spt5* mutants. p.adj < 0.05 and $\log_2$FC > 0 or $\log_2$FC < 0.

Figure 4. Mutations disrupting Paf1C recruitment to RNAPII rescue the inviability of *swd2*Δ and *ref2*Δ mutants.

(A) UCSC genome browser tracks showing transposon coverage in the *SWD2* gene in WT or *spt5* mutant backgrounds. Rep numbers indicate independent biological replicates. For some biological replicates, multiple technical replicates were tested.

(B) Tetrad dissection of yeast diploids heterozygous for *spt5-S1-15A* and *ref2*Δ or *swd2*Δ.

(C-E) Colony size quantification of yeast tetrad dissections from diploids heterozygous for *ref2*Δ and/or *swd2*Δ with *spt5* mutations (C), Paf1C mutations (D), or Paf1C recruitment-defective mutations (E). WT, *ref*Δ, and *swd2*Δ single mutant colonies from all dissections are plotted for each graph. Bars represent mean colony size with standard deviation. Colony sizes were quantified in pixels from scanned images after 3 days of growth on YPD. Black dotted line indicates mean colony size for WT strains.

(F) Yeast spot dilution growth assay showing the effect of *RTF1* complementation in the indicated strains. For the plate shown on the right, galactose was added to induce *RTF1* expression from the *GAL1* promoter on the plasmid. EV=empty vector.

Figure 5. Ref2 and Swd2 are required for chromatin association of Glc7 at the 3' ends of genes.

(A) Western blot analysis of strains used for genomic experiments. Black bar indicates the same strains/replicates. n=3

(B) Metaplots of mean spike-in normalized ChIP-seq data for the indicated proteins. The same color code is used in (C) and (E). n=2

(C) 4tU-seq sense strand and ChIP-seq signal at a highly transcribed locus, *CDC19*. Black arrows indicate Glc7 enrichment peak.

(D) Differential heatmaps of ChIP-seq signal for the indicated proteins. Genes are divided into quartiles based on Rpb1 occupancy (highest occupancy in quartile 1) in WT (KY4803) and sorted by gene length. Dashed line indicates CPS.

(E) Metaplot showing mean spike-in normalized 4tU-seq signal for the sense strand. Line colors are defined in (B). n=2

(F) Heatmap showing $\log_2$-fold change in 4tU-seq signal for the sense strand, centered at the CPS.

(G) Boxplot of $\log_2$-fold change in readthrough index stratified by quartiles of genic RNAPII occupancy, determined as in (D).

Figure 6. Glc7 is required for the dissociation of Paf1C from RNAPII at the CPS.

(A) Western blot analysis showing abundance of indicated proteins and histone modifications in the anchor-away strain (*GLC7-3xHA-FRB*) and a control strain (*GLC7-3xHA*). Cells were untreated (Pre) or treated with DMSO or rapamycin (Rapa, 1μg/mL) for 1 hr. n≥3

(B) Metaplots of mean spike-in normalized ChIP-seq signal for the indicated proteins. n=2

(C) ChIP-seq signals for the indicated proteins at a highly transcribed locus, *PDC1*. Anti-Myc serves as an unrelated antibody control.

(D) Differential heatmaps of ChIP-seq data from the *GLC7-3xHA-FRB* strain treated with rapamycin or DMSO and centered at the CPS.

Figure 7. Paf1C mutations strongly suppress transcriptional readthrough caused by nuclear depletion of Glc7.

(A) Metaplots of mean spike-in normalized 4tU-seq signal for the sense strand. Cells were treated with DMSO or rapamycin (1µg/mL) for 1 hr. $n \geq 2$

(B) Heatmap showing $\log_2$-fold change in 4tU-seq signal for the sense strand centered at the CPS upon Glc7 anchor-away.

(C) 4tU-seq sense signal at a highly transcribed locus, *RPL26A*.

(D) Boxplot showing $\log_2$-fold change in readthrough index stratified by genic RNAPII occupancy in quartiles as in Figure 5G.

(E) Colony size quantification of yeast tetrad dissection. Diploids heterozygous for *swd2*Δ and *rpb1* mutations that affect RNAPII catalytic rate were sporulated and haploid progeny were imaged for quantification after 3 days of growth on YPD.

(F) Model of the Glc7-mediated elongation-termination transition. Dephosphorylation of the Spt5 CTR (and possibly other substrates) by Glc7 triggers dissociation of Paf1C from RNAPII and proper mRNA cleavage and transcription termination under WT conditions. Upon Glc7 nuclear depletion, the Spt5 CTR is hyperphosphorylated, leading to Paf1C retention beyond the CPS and transcriptional readthrough. Yellow circles represent phosphates on the Spt5 CTR.

RESOURCE TABLE

REAGENT or RESOURCE	SOURCE	IDENTIFIER
Antibodies		
Rabbit α-Spt5 (Central)	Hartzog lab	N/A
Rabbit α-phospho-Spt5	Hahn lab; Liu *et al*.[12]	N/A
Rabbit α-Rtf1	Squazzo *et al*.[35]	N/A
Mouse α-Rpb1 CTD (8WG16)	BioLegend	Cat# 664906; RRID: AB_2565554
Rabbit α-Rpb1 core (Y80)	Santa Cruz Biotechnology	Cat# SC-25758
Rat α-Rpb1 CTD-Ser2P (3E10)	Active Motif	Cat# 61984; RRID: RRID:AB_2687450
Rat α-Rpb1 CTD-Ser5P (3E8)	Active Motif	Cat# 61086; RRID:AB_2687451
Mouse α-HA (12CA5)	Roche	Cat# 11666606001; RRID: AB_514506
Rabbit α-G6PDH	Sigma-Aldrich	Cat# A9521; RRID: AB_258454
Rabbit α-HSV	Sigma-Aldrich	Cat# H6030; RRID: AB_439691
Rabbit α-Spt6	Formosa lab; McCullough *et al*.[121]	RRID: AB_2687439
Rabbit α-H3 K4me1	Millipore	Cat# 07-436; RRID: AB_310614
Rabbit α-H3 K4me3	Active Motif	Cat# 39159; RRID: AB_2615077
Rabbit α-H2B K123ub	Cell Signaling Technology	Cat# 5546; RRID: AB_10693452
Mouse HA-antibody (F-7) conjugated beads	Santa Cruz Biotechnology	Cat# sc-7392 AC
Mouse α-FLAG M2 affinity gel	Millipore	Cat# A2220; RRID:AB_10063035
Mouse α-FLAG (M2)	Sigma-Aldrich	Cat# F3165; RRID:AB_259529
Rabbit α-Myc	John Woolford lab	N/A
Donkey α-Rabbit IgG HRP	Cytiva	Cat# NA934; RRID: AB_772206

Goat α-Rat IgG HRP	Cell Signaling Technology	Cat# 7077S; RRID: AB_10694715
Sheep α-Mouse IgG HRP	Cytiva	Cat# NA931; RRID: AB_772210
Chemicals, peptides, and recombinant proteins		
5-phenyl-indole-3-acetic acid	Tocris Bioscience	Cat# 7392
3-indoleacetic acid	Sigma-Aldrich	Cat# I3750
Rapamycin	MedChemExpress	Cat# HY-10219
SuperSignalTM West Pico PLUS Chemiluminescent Substrate	Thermo Fisher	Cat# 34580
4-thiouracil	Sigma-Aldrich	Cat# 440736-1G
Dynabeads MyOne Streptavidin C1	Invitrogen	Cat# 65001
MTSEA biotin-X	Biotium	Cat# 90066
5-fluoroorotic acid	Gold Biotechnology	Cat# F-230-10
AMPure XP	Beckman Coulter	Cat# A63881
Critical commercial assays		
NEBNext® Ultra™ II DNA Library Prep Kit for Illumina	NEB	Cat# E7645S/L
NEBNext® Multiplex Oligos for Illumina	NEB	Cat# E6440S/L
Pierce™ BCA Protein Assay Kit	Thermo Scientific	Cat# 23227
nProtein A Sepharose™ 4 Fast Flow beads	Cytiva	Cat# 17-5280-01
Protein G Sepharose™ 4 Fast Flow beads	Cytiva	Cat# 17-0618-01
QIAquick PCR Purification kit	Qiagen	Cat# 28106
Universal Plus™ Total RNA-Seq with NuQuant	Tecan Genomics	Cat# 0361-A01
UPlus Total AnyDeplete® Custom Probe Mix, *S. cerevisiae*	Tecan Genomics	Cat# S02714
UPlus Total RNA AnyDeplete® Module	Tecan Genomics	Cat# 0370-A01
RNeasy MinElute Cleanup Kit	Qiagen	Cat# 74204
Experimental models: Organisms/strains		
S. cerevisiae, see Table S1 for strain list	This study	N/A
K. lactis, see Table S1 for strain list	Nathan Clark lab, Kevin Struhl lab	N/A
S. pombe, see Table S1 for strain list	Fred Winston lab, this study	N/A

Oligonucleotides		
See Table S2 for oligonucleotide list	This study	N/A
Recombinant DNA		
Plasmid: *hphMX-tetO-pCYC1-3xminiAID*	Tanaka *et al*.[122]	pST1872
Plasmid: *pFA6a-3xHA-NatMX6*	Van Driessche *et al*.[123]	EuroScarf: P30412
Plasmid: *pFA6a-FRB-KanMX6*	Haruki *et al*.[90]	EuroScarf: P30578
Plasmid: *pFA6a-3xHA-KanMX6*	Longtine *et al*.[124]	Addgene: 39295
Plasmid: Transposase; *miniDs*; *ADE2*	Kornmann lab; Michel and Kornmann[77]	pBK549
Plasmid: pYES2=*pGAL1-3xHA-RTF1*, 2μ, *URA3*	This study	KB1001a
Plasmid: pML107=*CAS9*, gRNA, *2μ*, *LEU2*	Laughery *et al*.[125]	Addgene: 67639
Software and algorithms		
Prism	GraphPad	N/A
R version 4.2.1	N/A	https://www.r-project.org/
Bowtie2 version 2.4.5	Langmead and Salzberg[126]	http://bowtie-bio.sourceforge.net/bowtie2/index.shtml; RRID:SCR_016368
SAMtools version 1.14	Li *et al*.[127]	*http://htslib.org/; RRID:SCR_002105*
BAMtools version 2.5.1	Barnett *et al*.[128]	https://github.com/pezmaster31/bamtools/wiki; RRID:SCR_015987
BEDTools version 2.31.0	Quinlan and Hall[129]	https://github.com/arq5x/bedtools2; RRID:SCR_006646
Deeptools version 3.3.0	Ramírez *et al*.[130]	https://deeptools.readthedocs.io/en/develop/; RRID:SCR_016366

Sambamba version 0.8.1	Tarasov *et al*.[131]	https://github.com/biod/sambamba; RRID:SCR_024328
GNU Parallel	Tange[132]	https://www.gnu.org/software/parallel/
HISAT2 version 2.2.1	Kim *et al*.[133]	http://ccb.jhu.edu/software/hisat2/index.shtml; RRID:SCR_015530
DESeq2	Love *et al*.[134]	https://bioconductor.org/packages/release/bioc/html/DESeq2.html; RRID:SCR_015687
clusterProfiler	Yu *et al*.[135]	http://bioconductor.org/packages/release/bioc/html/clusterProfiler.html; RRID:SCR_016884
featureCounts	Liao *et al*.[136]	https://subread.sourceforge.net/featureCounts.html; RRID:SCR_012919
Fastp version 0.19.6	Chen[137]	https://github.com/OpenGene/fastp; RRID:SCR_016962
EBImage	Pau *et al*.[138]	https://bioconductor.org/packages/release/bioc/html/EBImage.html
ggplot2	Wickham[139]	https://cran.r-project.org/web/packages/ggplot2/index.html; RRID:SCR_014601

BioRad Image Lab	https://www.bio-rad.com/en-us/product/image-lab-software?ID=KRE6P5E8Z	N/A
UCSC Genome Browser	Perez *et al*.[140]	http://genome.ucsc.edu
Integrative Genomics Viewer	Robinson *et al*.[141]	http://www.broadinstitute.org/igv/; RRID:SCR_011793
SATAY data analysis code	Michel *et al*.[76]	https://kornmann.bioch.ox.ac.uk/satay/index.html

MATERIALS AND METHODS

Yeast strains and growth conditions

Saccharomyces cerevisiae strains used in this study are isogenic to FY2, a *GAL2*$^{+}$ derivative of S288C[142]. Mutant strains were generated using one-step integrative transformation or derived from genetic crosses.[143] Yeast transformations were performed following the lithium acetate transformation protocol.[143] For gene replacements, DNA fragments containing a selection marker and homology arms for recombination were amplified by PCR from plasmids or yeast deletion collection strains as a DNA template. Tagging of *GLC7* with *3xHA* or *3xHA-FRB* at either the C- or N-terminus was done using CRISPR/Cas9 as described previously.[125] All mutations were confirmed by PCR and/or Sanger sequencing. Sequences of oligonucleotides used for strain constructions are available upon request. Plasmids used in this study are listed in the Resources table.

S. cerevisiae, *K. lactis,* and *S. pombe* strains were grown at 30˚C in YPD medium supplemented with 400 μM tryptophan (YPD+W) or synthetic complete (SC) dropout medium.[143] For auxin-induced depletion of mAID-Spt5, yeast cultures at an OD_{600} of ~0.5 (~10^7 cells/mL) were treated with 5-phenyl-indole-3-acetic acid (5-Ph-IAA, Tocris Bioscience, 7392) at a final concentration of 5 μM or an equivalent amount of vehicle (DMSO) and incubated at 30˚C for the indicated time. For Glc7 anchor-away experiments, 1 μg/mL rapamycin (MedChemExpress, HY-10219) or an equivalent amount of vehicle (DMSO) was added to the yeast cultures. All cultures harvested for western blots were quenched with cold methanol (stored at -20˚C) at ~33% v/v final concentration to stop treatment at the indicated timepoint and preserve post-translational modifications.[144] Cells were washed once with water before centrifugation, and cell pellets were flash frozen in liquid nitrogen.

Yeast serial dilution spot growth assay

Yeast cells were grown at 30˚C in YPD+W to stationary phase and diluted to an OD_{600} of 1.0 (~2 x 10^7 cells/mL) in water in a 96-well plate. Cell suspensions were serially diluted 5-fold in water to a final volume of 160 µL. A 96-well plate replicator (Sigma-aldrich, R2383-1EA) was used to spot cells onto the indicated media. Plates were incubated at 30˚C and scanned (Epson Perfection V600 photo) at ~24-hour intervals.

Western blot analysis

Protein extracts were prepared from methanol-quenched cells (see above) equivalent to an OD_{600} of 10 using the post-alkaline method[145] with minor modifications. Briefly, cell pellets were resuspended in 100 µL of either water or 2x PhosSTOP phosphatase inhibitor stock (Roche, 04906845001) and treated with 100 µL of 0.2 M NaOH for 5 min at room temperature before spinning at 14,000 rpm for 5 min. The resulting pellets were resuspended in 200 µL of 1x SDS-PAGE loading buffer (62.5 mM Tris-HCl pH 6.8, 2% SDS, 10% glycerol, 0.1% bromophenol blue, 5% beta-mercaptoethanol (added fresh)) and boiled at 100˚C for 5 min. Boiled samples were spun at 14,000 rpm for 5 min and the supernatant was transferred to a fresh microcentrifuge tube. Proteins were resolved on 8% or 15% SDS-polyacrylamide Tris-glycine gels and transferred to nitrocellulose membranes. Nitrocellulose membranes were blocked in 5% dry milk in 1X TBST for 1 hour at room temperature. The membrane was then incubated in 5% milk in 1X TBST containing 0.02% sodium azide with primary antibody overnight at 4˚C. The primary antibodies used were: anti-Rpb1 CTD (8WG16, BioLegend, 664906, 1:500), anti-Rpb1 core (Y80, Santa Cruz, SC-25758, 1:1000), anti-Ser2P (3E10, Active Motif, 61984, 1:1000), anti-Ser5P (3E8, Active Motif, 61086, 1:500), anti-Spt5 central (gift from Grant Hartzog, 1:1000), anti-Spt6 (gift from Tim Formosa, McCullough *et al.*,[121] 1:1000), anti-Rtf1 (Squazzo *et al.*,[35] 1:2500), anti-HSV (Sigma-Aldrich, H6030, 1:2000), anti-FLAG (Sigma-Aldrich, F3165, 1:3000),

anti-HA (Roche, 11666606001, 1:3000), anti-phospho-Spt5 (gift from Steven Hahn, Liu *et al*.,[12] 1:340), anti-H2BK123ub (Cell Signaling, 5546, 1:1000), anti-H3K4me1 (Millipore, 07-436, 1:2000), anti-H3K4me3 (Active Motif, 39159, 1:2000) and anti-G6PDH (Sigma-Aldrich, A9521, 1:20,000). The anti-Spt5 central antibody was directed against a maltose-binding protein (MBP)-Spt5 (amino acids 402-677) fusion protein. This protein was expressed from plasmid pGH79, using an MBP protein fusion and purification system from New England Biolabs (Beverly, MA), according to their instructions. Rabbits were immunized with the MBP-Spt5 fusion protein by Cocalico Biologicals (Reamstown, PA). After incubation with the primary antibody, membranes were washed with 1x TBST and incubated with secondary antibody (1:5000 dilution of HRP-conjugated anti-mouse (Cytiva, NA931) or anti-rabbit (Cytiva, NA934)) for 1 hour at room temperature. Proteins were visualized using Pico PLUS chemiluminescent substrate (Thermo Fisher, 34580) on a ChemiDoc XRS imaging platform (BioRad, Hercules, CA).

ChIP-seq sample preparation, library construction, and data processing

Chromatin immunoprecipitation (ChIP) was performed with 250 mL cultures of yeast cells grown to an OD_{600} of 1.0 (~2 x 10^7 cells/mL) as described previously.[46] When yeast cultures were exposed to treatments (*e.g.* auxin), formaldehyde was added at the indicated timepoint post treatment. For all ChIP experiments, *S. cerevisiae* chromatin was mixed with spike-in chromatin at a 1:10 ratio (spike-in chromatin : *S. cerevisiae* chromatin) based on protein concentration (Pierce BCA protein assay kit; Thermo Fisher Scientific, 23227). Different sources of spike-in chromatin were used for different IP reactions depending on the antibody cross-reactivity, which was confirmed by western blotting. *Schizosaccharomyces pombe* KP10 chromatin was used for 8WG16 (BioLegend, 664906, 6 µL/1350 µg) and HSV (Sigma-Aldrich, H6030, 5 µL/1350 µg) IPs in Figures 1 and 2, while *S. pombe* KP06 chromatin was used for 8WG16 (6 µL/1350 µg or 4 µL/900 µg), HA (Santa-Cruz, sc-7382 AC, 60 µL/1350 µg or 60 µL/1800 µg) and Myc (non-

specific IgG control, gift from John Woolford, 5 µL/900 µg) IPs in Figures 5 and 6. *Kluyveromyces lactis* KL01 chromatin was added to IP reactions for Spt5 central (gift from Grant Hartzog, 2 µL/900 µg or 3 µL/1350 µg), Spt6 (gift from Tim Formosa, McCullough *et al*.,[121] 8 µL/1350 µg or 6 µL/900 µg) and Rtf1 (Squazzo *et al*.,[35] 4 µL/1350 µg or 3 µL/900 µg), while *K. lactis* KL02 chromatin was used for Rpb3-FLAG (Millipore, A2220, 100 µL slurry/900 µg) IPs. IP reactions were incubated at 4˚C overnight on an end-over-end roller. Pre-equilibrated 50% slurry of protein A or G beads (Cytiva, 17-5280-01 or 17-0618-01, 80 µL/1350 µg or 60 µL/900 µg) was added, and samples were incubated at room temperature for 1 hour with rotation. Beads were washed as previously described.[46] To elute DNA, beads were incubated with 125 µL of elution buffer (50 mM Tris pH 8, 10 mM EDTA, 1% SDS) at 65˚C for 10 min. After washing beads with another 125 µL of TE buffer (10 mM Tris pH 8, 1 mM EDTA) to a total of 250 µL eluate, samples were treated with 20 µL of 10 mg/mL pronase (Roche, 10165921001) at 42˚C for 2 hours. To reverse crosslinks, samples were incubated at 65˚C overnight. DNA was purified using the QIAquick PCR Purification Kit (Qiagen, 28106). ChIP-seq libraries were prepared using the NEBNext Ultra II DNA kit (NEB, E7645S/S) and multiplex oligos (NEB, E6440S/L). AMPure XP beads (Beckman Coulter, A63881) were used for DNA library clean-up. Libraries were paired-end sequenced (2x50 bp) on the Illumina NextSeq 2000 platform by the University of Pittsburgh Health Sciences Sequencing Core at UPMC Children's Hospital of Pittsburgh.

Reads were mapped to a concatenated hybrid genome of *S. cerevisiae* (SacCer3) and *K. lactis* (ASM251v1) or *S. pombe* (ASM294v2) using bowtie2 version 2.4.5 (-p 12 -q -k 2 --no-mixed --no-discordant --no-overlap).[126] Sam files were then converted to bam files with Samtools,[127] and multimapping reads were filtered out with Sambamba view (-h -t 8 -F "[XS] == null" -f bam).[131] PCR duplicate reads were removed with Samtools markdup. Spike-in normalization factors (NormFactor) were calculated as described previously.[46,146] Coverage for each base pair of the *S. cerevisiae* genome was computed using bamCoverage (--scaleFactor

[NormFactor], --outFileFormat bigwig --binSize 1 --extendReads --numberOfProcessors "max") from deeptools (version 3.3.0)[130] to apply spike-in normalization. For RPKM normalization, --normalizeUsing RPKM option was used instead of –scaleFactor. Metaplots and heatmaps were visualized using the deeptools suite. Genes with no coverage detected in WT (KY4803) ChIP-seq datasets were removed from the non-overlapping protein-coding gene (n=3087) annotation[118] bed file and the remaining genes (n=3057) were used for all data visualization. All metaplot and heatmaps were generated from data in 10-nt bins.

4tU-seq sample preparation, library construction, and data processing

The protocols for 4-thiouracil (4tU) labeling and cell harvesting were adapted from.[38,147] First, strain/mutant-specific linear regression equations of OD_{600} versus cell number was determined by counting cells under a microscope with a hemocytometer. At the time of the harvest, the number of cells was extrapolated from a specific OD_{600} using the linear equation. For all cell harvests, a culture-volume equivalent of 5×10^8 or 6×10^8 total cells was transferred to a fresh tube for 4tU labeling. Cells were labelled with 4-thiouracil (Sigma-Aldrich, 440736-1G) at a 5 mM final concentration for 5 min at room temperature with shaking and quenched with cold methanol (stored at -20˚C) at 33% v/v final concentration to halt 4tU labeling. For mutant and WT strains, cultures were grown to an OD_{600} of ~1.0 before 4tU labeling. For strains with treatment, cultures were grown to an OD_{600} of ~0.7 before being split and treated, and 4tU was added at the indicated timepoint post treatment for 5 min labeling. Spike-in strain *S. pombe* (KP10) was grown to an OD_{600} of 1.0 and labelled with 4tU for 10 min. Methanol-quenched cultures were centrifuged at 3000 rpm for 3 min at 4˚C, and cell pellets were washed once with ice cold water before being flash frozen in liquid nitrogen. For all cultures, cells were also counted under a microscope using a hemocytometer to record the precise cell concentration at the time of harvest, which was used for post-hoc cell count normalization as described below.

S. cerevisiae cells were mixed with spike-in *S. pombe* cells at a 10:1 ratio (*S. cerevisiae*:*S. pombe*) by cell number. For Glc7 anchor-away samples including two replicates of WT, *paf1*Δ or *rtf1*Δ strains, a *S. cerevisiae* cell suspension volume equivalent to 5 x 10^8 cells based on the cell count at the time of harvest was used as the input. For all other strains including another two replicates of WT Glc7 anchor-away, the entire harvested cell pellet (equivalent to 6 x 10^8 cells) was used as the input for RNA extraction. RNA was extracted from the cell mixture using a hot acid phenol extraction protocol as described previously.[38] 4tU-labeled nascent RNA biotinylation and isolation were performed as described previously.[38,147] Briefly, RNA biotinylation was carried out on 50 µg of total RNA using 10 µg/mL MTSEA Biotin-XX (Biotium, 90066; 50 µg/mL stock prepared in dimethyl formamide) in a total volume of 400 µL biotinylation buffer (20 mM HEPES pH 7.4, 1 mM EDTA) for 30 min at room temperature on a rotator, protected from light. In parallel, magnetic MyOne Streptavidin C1 beads (Invitrogen, 65001) were pre-equilibrated in high salt buffer (100 mM Tris, pH 7.4, 10 mM EDTA, 1 M NaCl, 0.05% Tween-20) and blocked in blocking buffer (high salt buffer, 40 ng/µL glycogen) for 1 hour. After blocking, beads were washed in high salt buffer and resuspended in the original volume of the bead slurry in high salt buffer. Unreacted biotin was removed from the biotinylation reaction using phenol extraction and the RNA was purified with isopropanol precipitation. The RNA was resuspended in 100 µL of nuclease-free water and incubated with 80 µL of the blocked beads for 15 min with shaking. The biotinylated RNA-bound beads were washed with high salt buffer on a magnetic stand, and RNA was eluted in 25 µL of elution buffer (100 mM DTT, 20 mM HEPES pH 7.4, 1 mM EDTA, 100 mM NaCl, and 0.05% Tween-20) for 15 min twice to a total of 50 µL eluate. The RNA eluate was concentrated using an RNeasy MinElute cleanup kit (Qiagen, 74204). 4tU-seq libraries were prepared using a Universal Plus Total RNA-seq with NuQuant kit (Tecan, 0361-A01), UPlus Total RNA AnyDeplete module (Tecan, 0370-A01) and UPlus Total AnyDeplete Custom Probe Mix for S. *cerevisiae* (Tecan, S02714). Libraries were sequenced

(paired-end, 100 bp) on the Illumina NextSeq 2000 platform by the University of Pittsburgh Health Sciences Sequencing Core at UPMC Children's Hospital of Pittsburgh.

Reads were first processed with Fastp (--low_complexity_filter --correction --overrepresentation_analysis)[137] and mapped to a concatenated hybrid genome of *S. cerevisiae* (SacCer3) and *S. pombe* (ASM294v2) using HISAT2 version 2.2.1 (--rna-strandness FR --no-unal -k 2 -p 4).[133] Sam files were then converted to bam and duplicate reads were removed using the samtools suite.[127] *S. cerevisiae* and *S. pombe* reads were separated using Bamtools split[128] and Samtools merge. For spike-in normalization, *S. pombe* reads over coding features were counted with featureCounts[136] and the DESeq2 estimateSizeFactors()[134] function was used to generate spike-in size factors. Because the cell concentration of *S. cerevisiae* counted at the time of the harvest deviated from the number extrapolated from the linear fit by ±10%, we also applied cell count normalization to *S. cerevisiae* coverage for each base pair. The following formula was used to compute the normalization factor that takes into account both spike-in and cell count normalizations.

$$NormFactor = \frac{1}{Spike-in\ size\ factor} \times \frac{1}{\frac{(Total\ cell\ number\ of\ mutant)}{(Total\ cell\ number\ of\ WT\ (KY4803\ Rep\ 1))}}$$

Four replicates of WT Glc7 anchor-away were sequenced in total. Two replicates of WT Glc7 anchor-away were normalized post-hoc using spike-in and cell count as above. For the other two replicates of WT Glc7 anchor-away along with *paf1*Δ and *rtf1*Δ strains, only spike-in normalization was applied to *S. cerevisiae* coverage, because the total number of cells were normalized using harvested cell count information before going into RNA extraction and library build. Bam files were converted to stranded bigwig files using bamCoverage (--scaleFactor [NormFactor] --outFileFormat bigwig --binSize 1 --numberOfProcessors "max") from deeptools (version 3.3.0).[130] Metaplots and heatmaps were visualized in 10-nt bins using the same gene annotation set that was used for ChIP-seq and the deeptools suite.

SATAY transposon library preparation and data processing

Transposition libraries of the *spt5* mutant strains were generated as described previously.[76] Briefly, 200 mL of freshly prepared SD-Ura + 2% raffinose + 0.2% dextrose media was inoculated with the *ade2*Δ *spt5* mutant yeast strains transformed with pBK549 plasmid,[77] which was scraped from a patch grown on a selective medium plate, at a final OD_{600} of 0.16-0.18. Individual transformants are considered biological replicates. The cultures were grown to saturation for 18 to 48 hours at 30˚C with shaking. Cells were spun down for 2 min at 1700 x g, 20˚C, and concentrated in the same media at a final OD_{600} of 39. A cell suspension equivalent to an OD_{600} of 7.8 was spread per plate on ~50-60 SD-Ade + 2% galactose plates using glass spreaders. Plates were incubated for 18-20 days at 30˚C. All colonies on the plates were then scraped off the plates using 200 µL of sterile water per plate and pooled. The pooled cell suspension was used to inoculate 2 L of SD-Ade + 2% dextrose culture at an initial density of 2.5×10^6 cells/mL, which was then grown to saturation at 30˚C with shaking for 24-48 hours. The saturated culture was harvested by centrifugation at 1600 x g for 5 minutes and the cell pellet was washed with water and flash frozen in liquid nitrogen as ~500 mg aliquots. Genomic DNA was extracted from a 500 mg cell pellet and 2 µg of extracted gDNA was digested with restriction enzymes *NlaIII* and *DpnII*, separately. The digested DNA was circularized using T4 ligase and then amplified by PCR with custom P5 and P7 index primers. Index 1 (i7) adapter sequences from TruSeq kits for Illumina were used as index sequences. Libraries were sequenced (single-end, 150 bp) with custom sequencing primers on the Illumina NextSeq 500 platform by the University of Pittsburgh Health Sciences Sequencing Core at UPMC Children's Hospital of Pittsburgh.

Yeast tetrad colony size quantification

The colony sizes on yeast tetrad dissection plates were quantified in pixels using a custom R script that utilizes EBImage R package.[138] Fitness and deviation scores were calculated using the quantified colony sizes as described previously.[78]

SATAY analysis

The sequencing data were analyzed using a custom R script obtained from the lab of Benoit Kornmann (University of Oxford). A resulting parameter, number of transposons per gene (tnpergene), was normalized to the total number of transposons mapped in the library and multiplied by 1 million for simplicity. Normalized tn/gene data of technical replicates (separate sequencing runs for the same transformant or library) of the same biological replicate were averaged and used for all downstream analyses. Raw bed files containing all mapped transposons were uploaded to UCSC genome browser for visualization. Differential transposition analysis was performed using DESeq2[134] and genes that had significantly different transposon coverage were defined using the cutoff of $p.adj \leq 0.05$. ClusterProfiler[135] was used to perform Gene Ontology (GO) term enrichment analysis.[120]

Elongation index

Elongation index[71] was computed by taking the ratio of 4tU-seq over Pol II ChIP-seq (either Rpb3-FLAG or 8WG16) coverage in 25-nt bins using bigwigCompare from the deeptools suite.[130] Heatmap and metaplot representations of elongation index were visualized using deeptools.

Splicing efficiency

4tU-seq total read coverage (including both spliced and unspliced) overlapping +1 base (5' splice site)[38,148] of each annotated chromosomal intron feature from *S. cerevisiae* gff file from SGD[149] was determined using bedtools coverage (-s -a -counts). Unspliced read coverage was determined with an additional -split option. Introns with spliced read coverage below an arbitrary threshold of 5 were excluded to avoid artifacts originating from low gene expression level. Splicing efficiency was calculated by dividing the read coverage of spliced reads by the total read coverage of spliced and unspliced reads per protein-coding gene intron.

Completion score

4tU-seq read density overlapping 200 bp windows, positioned 100 bp downstream of the TSS (proximal) or upstream of the CPS (distal), for the non-overlapping gene set (described above) was determined using multiBigwigSummary BED-file command. Only reads aligning on the sense strand were considered. Completion score was calculated by dividing distal read coverage by proximal read coverage and computing the $\log_2$ fold change.[38,75]

Readthrough index

4tU-seq read density overlapping 150 bp (50 bp for snoRNAs) windows immediately upstream (pre-CPS) or downstream (readthrough) of the CPS of the non-overlapping gene set was computed by multiBigwigSummary BED-file command. Readthrough index was calculated as the $\log_2$ fold change of readthrough read density compared to pre-CPS signal.[75]

Statistical analysis and data reproducibility

All genomic experiments were performed in biological duplicate, except for 4tU-seq analysis of the WT Glc7 anchor-away strain for which four replicates were included in Figure 7. Pearson's correlation analysis was used to assess replicate reproducibility. Each biological replicate is a pure yeast culture derived from a single colony. For calculations of splicing efficiency, completion score and readthrough index, *p*-values were generated using Mann-Whitney U test (wilcox.test in R) with FDR correction. For SATAY, at least two biological replicates (independent transformants) with one to three technical replicates were analyzed for all strains. Principal component analysis (PCA) was used to assess SATAY replicate reproducibility. For yeast tetrad dissections, at least two independently generated diploid strains were assessed. For the colony size measurements, at least nine individual colonies were analyzed for each genotype. All western blots were performed in biological triplicate or more, except for *glc7-T152K* mutant which had two replicates, and *p*-values associated with the quantification were calculated in GraphPad Prism as indicated in the figure legends.

REFERENCES

1. Aoi, Y., and Shilatifard, A. (2023). Transcriptional elongation control in developmental gene expression, aging, and disease. Mol. Cell *83*, 3972-3999. 10.1016/j.molcel.2023.10.004.
2. Farnung, L. (2025). Chromatin Transcription Elongation - A Structural Perspective. J. Mol. Biol. *437*, 168845. 10.1016/j.jmb.2024.168845.
3. Lopez Martinez, D., and Svejstrup, J.Q. (2025). Mechanisms of RNA Polymerase II Termination at the 3'-End of Genes. J. Mol. Biol. *437*, 168735. 10.1016/j.jmb.2024.168735.
4. Rodriguez-Molina, J.B., West, S., and Passmore, L.A. (2023). Knowing when to stop: Transcription termination on protein-coding genes by eukaryotic RNAPII. Mol. Cell *83*, 404-415. 10.1016/j.molcel.2022.12.021.
5. Harlen, K.M., and Churchman, L.S. (2017). The code and beyond: transcription regulation by the RNA polymerase II carboxy-terminal domain. Nat. Rev. Mol. Cell. Biol. *18*, 263-273. 10.1038/nrm.2017.10.
6. Sun, R., and Fisher, R.P. (2025). The CDK9-SPT5 Axis in Control of Transcription Elongation by RNAPII. J. Mol. Biol. *437*, 168746. 10.1016/j.jmb.2024.168746.
7. Kim, D.K., Inukai, N., Yamada, T., Furuya, A., Sato, H., Yamaguchi, Y., Wada, T., and Handa, H. (2003). Structure-function analysis of human Spt4: evidence that hSpt4 and hSpt5 exert their roles in transcriptional elongation as parts of the DSIF complex. Genes Cells *8*, 371-378. 10.1046/j.1365-2443.2003.00638.x.
8. Wada, T., Takagi, T., Yamaguchi, Y., Ferdous, A., Imai, T., Hirose, S., Sugimoto, S., Yano, K., Hartzog, G.A., Winston, F., et al. (1998). DSIF, a novel transcription elongation factor that regulates RNA polymerase II processivity, is composed of human Spt4 and Spt5 homologs. Genes Dev. *12*, 343-356. 10.1101/gad.12.3.343.
9. Mayer, A., Lidschreiber, M., Siebert, M., Leike, K., Soding, J., and Cramer, P. (2010). Uniform transitions of the general RNA polymerase II transcription complex. Nat. Struct. Mol Biol *17*, 1272-1278. 10.1038/nsmb.1903.
10. Evrin, C., Serra-Cardona, A., Duan, S., Mukherjee, P.P., Zhang, Z., and Labib, K.P.M. (2022). Spt5 histone binding activity preserves chromatin during transcription by RNA polymerase II. EMBO J. *41*, e109783. 10.15252/embj.2021109783.
11. Hartzog, G.A., and Fu, J. (2013). The Spt4-Spt5 complex: a multi-faceted regulator of transcription elongation. Biochim Biophys Acta *1829*, 105-115. 10.1016/j.bbagrm.2012.08.007.
12. Liu, Y., Warfield, L., Zhang, C., Luo, J., Allen, J., Lang, W.H., Ranish, J., Shokat, K.M., and Hahn, S. (2009). Phosphorylation of the transcription elongation factor Spt5 by yeast Bur1 kinase stimulates recruitment of the PAF complex. Mol. Cell. Biol. *29*, 4852-4863. 10.1128/MCB.00609-09.
13. Parua, P.K., Booth, G.T., Sanso, M., Benjamin, B., Tanny, J.C., Lis, J.T., and Fisher, R.P. (2018). A Cdk9-PP1 switch regulates the elongation-termination transition of RNA polymerase II. Nature *558*, 460-464. 10.1038/s41586-018-0214-z.
14. Yamada, T., Yamaguchi, Y., Inukai, N., Okamoto, S., Mura, T., and Handa, H. (2006). P-TEFb-mediated phosphorylation of hSpt5 C-terminal repeats is critical for processive transcription elongation. Mol. Cell *21*, 227-237. 10.1016/j.molcel.2005.11.024.
15. Zhou, K., Kuo, W.H., Fillingham, J., and Greenblatt, J.F. (2009). Control of transcriptional elongation and cotranscriptional histone modification by the yeast BUR kinase substrate Spt5. Proc. Natl. Acad. Sci. U S A *106*, 6956-6961. 10.1073/pnas.0806302106.

16. Pei, Y., and Shuman, S. (2003). Characterization of the *Schizosaccharomyces pombe* Cdk9/Pch1 protein kinase: Spt5 phosphorylation, autophosphorylation, and mutational analysis. J. Biol. Chem. *278*, 43346-43356. 10.1074/jbc.M307319200.
17. Swanson, M.S., Malone, E.A., and Winston, F. (1991). *SPT5*, an essential gene important for normal transcription in *Saccharomyces cerevisiae*, encodes an acidic nuclear protein with a carboxy-terminal repeat. Mol. Cell. Biol. *11*, 3009-3019. 10.1128/mcb.11.6.3009-3019.1991.
18. Mayekar, M.K., Gardner, R.G., and Arndt, K.M. (2013). The recruitment of the *Saccharomyces cerevisiae* Paf1 complex to active genes requires a domain of Rtf1 that directly interacts with the Spt4-Spt5 complex. Mol. Cell. Biol. *33*, 3259-3273. 10.1128/MCB.00270-13.
19. Sun, R., and Fisher, R.P. (2025). Tripartite phosphorylation of SPT5 by CDK9 times pause release and tunes elongation rate of RNA polymerase II. Mol. Cell *85*, 1743-1759 e1745. 10.1016/j.molcel.2025.03.021.
20. Vos, S.M., Farnung, L., Linden, A., Urlaub, H., and Cramer, P. (2020). Structure of complete Pol II-DSIF-PAF-SPT6 transcription complex reveals RTF1 allosteric activation. Nat. Struct. Mol. Biol. *27*, 668-677. 10.1038/s41594-020-0437-1.
21. Wier, A.D., Mayekar, M.K., Heroux, A., Arndt, K.M., and VanDemark, A.P. (2013). Structural basis for Spt5-mediated recruitment of the Paf1 complex to chromatin. Proc. Natl. Acad. Sci. U S A *110*, 17290-17295. 10.1073/pnas.1314754110.
22. Doamekpor, S.K., Sanchez, A.M., Schwer, B., Shuman, S., and Lima, C.D. (2014). How an mRNA capping enzyme reads distinct RNA polymerase II and Spt5 CTD phosphorylation codes. Genes Dev. *28*, 1323-1336. 10.1101/gad.242768.114.
23. Pei, Y., and Shuman, S. (2002). Interactions between fission yeast mRNA capping enzymes and elongation factor Spt5. J. Biol. Chem. *277*, 19639-19648. 10.1074/jbc.M200015200.
24. Schneider, S., Pei, Y., Shuman, S., and Schwer, B. (2010). Separable functions of the fission yeast Spt5 carboxyl-terminal domain (CTD) in capping enzyme binding and transcription elongation overlap with those of the RNA polymerase II CTD. Mol Cell Biol *30*, 2353-2364. 10.1128/MCB.00116-10.
25. Suh, M.H., Meyer, P.A., Gu, M., Ye, P., Zhang, M., Kaplan, C.D., Lima, C.D., and Fu, J. (2010). A dual interface determines the recognition of RNA polymerase II by RNA capping enzyme. J. Biol. Chem. *285*, 34027-34038. 10.1074/jbc.M110.145110.
26. Wen, Y., and Shatkin, A.J. (1999). Transcription elongation factor hSPT5 stimulates mRNA capping. Genes Dev. *13*, 1774-1779. 10.1101/gad.13.14.1774.
27. Mayer, A., Schreieck, A., Lidschreiber, M., Leike, K., Martin, D.E., and Cramer, P. (2012). The Spt5 C-terminal region recruits yeast 3' RNA cleavage factor I. Mol. Cell. Biol. *32*, 1321-1331. 10.1128/MCB.06310-11.
28. Dollinger, R., and Gilmour, D.S. (2021). Regulation of Promoter Proximal Pausing of RNA Polymerase II in Metazoans. J. Mol. Biol. *433*, 166897. 10.1016/j.jmb.2021.166897.
29. Fong, N., Sheridan, R.M., Ramachandran, S., and Bentley, D.L. (2022). The pausing zone and control of RNA polymerase II elongation by Spt5: Implications for the pause-release model. Mol. Cell *82*, 3632-3645 e3634. 10.1016/j.molcel.2022.09.001.
30. Vos, S.M., Farnung, L., Boehning, M., Wigge, C., Linden, A., Urlaub, H., and Cramer, P. (2018). Structure of activated transcription complex Pol II-DSIF-PAF-SPT6. Nature *560*, 607-612. 10.1038/s41586-018-0440-4.
31. Vos, S.M., Farnung, L., Urlaub, H., and Cramer, P. (2018). Structure of paused transcription complex Pol II-DSIF-NELF. Nature *560*, 601-606. 10.1038/s41586-018-0442-2.

32. Wada, T., Takagi, T., Yamaguchi, Y., Watanabe, D., and Handa, H. (1998). Evidence that P-TEFb alleviates the negative effect of DSIF on RNA polymerase II-dependent transcription in vitro. EMBO J. *17*, 7395-7403. 10.1093/emboj/17.24.7395.
33. Krogan, N.J., Kim, M., Ahn, S.H., Zhong, G., Kobor, M.S., Cagney, G., Emili, A., Shilatifard, A., Buratowski, S., and Greenblatt, J.F. (2002). RNA polymerase II elongation factors of *Saccharomyces cerevisiae*: a targeted proteomics approach. Mol. Cell. Biol. *22*, 6979-6992. 10.1128/MCB.22.20.6979-6992.2002.
34. Mueller, C.L., and Jaehning, J.A. (2002). Ctr9, Rtf1, and Leo1 are components of the Paf1/RNA polymerase II complex. Mol. Cell. Biol. *22*, 1971-1980. 10.1128/MCB.22.7.1971-1980.2002.
35. Squazzo, S.L., Costa, P.J., Lindstrom, D.L., Kumer, K.E., Simic, R., Jennings, J.L., Link, A.J., Arndt, K.M., and Hartzog, G.A. (2002). The Paf1 complex physically and functionally associates with transcription elongation factors in vivo. EMBO J. *21*, 1764-1774. 10.1093/emboj/21.7.1764.
36. Zhu, B., Mandal, S.S., Pham, A.D., Zheng, Y., Erdjument-Bromage, H., Batra, S.K., Tempst, P., and Reinberg, D. (2005). The human PAF complex coordinates transcription with events downstream of RNA synthesis. Genes Dev. *19*, 1668-1673. 10.1101/gad.1292105.
37. Fetian, T., McShane, B.M., Horan, N.L., Shodja, D.N., True, J.D., Mosley, A.L., and Arndt, K.M. (2023). Paf1 complex subunit Rtf1 stimulates H2B ubiquitylation by interacting with the highly conserved N-terminal helix of Rad6. Proc. Natl. Acad. Sci. U S A *120*, e2220041120. 10.1073/pnas.2220041120.
38. Francette, A.M., and Arndt, K.M. (2024). Multiple direct and indirect roles of the Paf1 complex in transcription elongation, splicing, and histone modifications. Cell Rep. *43*, 114730. 10.1016/j.celrep.2024.114730.
39. Hou, L., Wang, Y., Liu, Y., Zhang, N., Shamovsky, I., Nudler, E., Tian, B., and Dynlacht, B.D. (2019). Paf1C regulates RNA polymerase II progression by modulating elongation rate. Proc. Natl. Acad. Sci. U S A *116*, 14583-14592. 10.1073/pnas.1904324116.
40. Van Oss, S.B., Shirra, M.K., Bataille, A.R., Wier, A.D., Yen, K., Vinayachandran, V., Byeon, I.L., Cucinotta, C.E., Heroux, A., Jeon, J., et al. (2016). The Histone Modification Domain of Paf1 Complex Subunit Rtf1 Directly Stimulates H2B Ubiquitylation through an Interaction with Rad6. Mol. Cell *64*, 815-825. 10.1016/j.molcel.2016.10.008.
41. Zumer, K., Maier, K.C., Farnung, L., Jaeger, M.G., Rus, P., Winter, G., and Cramer, P. (2021). Two distinct mechanisms of RNA polymerase II elongation stimulation in vivo. Mol. Cell *81*, 3096-3109 e3098. 10.1016/j.molcel.2021.05.028.
42. Simic, R., Lindstrom, D.L., Tran, H.G., Roinick, K.L., Costa, P.J., Johnson, A.D., Hartzog, G.A., and Arndt, K.M. (2003). Chromatin remodeling protein Chd1 interacts with transcription elongation factors and localizes to transcribed genes. EMBO J. *22*, 1846-1856. 10.1093/emboj/cdg179.
43. Tripplehorn, S.A., Shirra, M.K., Lardo, S.M., Marvil, H.G., Hainer, S.J., and Arndt, K.M. (2025). A direct interaction between the Chd1 CHCT domain and Rtf1 controls Chd1 distribution and nucleosome positioning on active genes. Nucleic Acids Res. *53*, gkaf816. 10.1093/nar/gkaf816.
44. Amrich, C.G., Davis, C.P., Rogal, W.P., Shirra, M.K., Heroux, A., Gardner, R.G., Arndt, K.M., and VanDemark, A.P. (2012). Cdc73 subunit of Paf1 complex contains C-terminal Ras-like domain that promotes association of Paf1 complex with chromatin. J. Biol. Chem. *287*, 10863-10875. 10.1074/jbc.M111.325647.
45. Ehara, H., Kujirai, T., Shirouzu, M., Kurumizaka, H., and Sekine, S.I. (2022). Structural basis of nucleosome disassembly and reassembly by RNAPII elongation complex with FACT. Science *377*, eabp9466. 10.1126/science.abp9466.

46. Ellison, M.A., Namjilsuren, S., Shirra, M.K., Blacksmith, M.S., Schusteff, R.A., Kerr, E.M., Fang, F., Xiang, Y., Shi, Y., and Arndt, K.M. (2023). Spt6 directly interacts with Cdc73 and is required for Paf1 complex occupancy at active genes in *Saccharomyces cerevisiae*. Nucleic Acids Res. *51*, 4814-4830. 10.1093/nar/gkad180.
47. Qiu, H., Hu, C., Gaur, N.A., and Hinnebusch, A.G. (2012). Pol II CTD kinases Bur1 and Kin28 promote Spt5 CTR-independent recruitment of Paf1 complex. EMBO J. *31*, 3494-3505. 10.1038/emboj.2012.188.
48. Cortazar, M.A., Sheridan, R.M., Erickson, B., Fong, N., Glover-Cutter, K., Brannan, K., and Bentley, D.L. (2019). Control of RNA Pol II Speed by PNUTS-PP1 and Spt5 Dephosphorylation Facilitates Termination by a "Sitting Duck Torpedo" Mechanism. Mol. Cell *76*, 896-908 e894. 10.1016/j.molcel.2019.09.031.
49. Eaton, J.D., Francis, L., Davidson, L., and West, S. (2020). A unified allosteric/torpedo mechanism for transcriptional termination on human protein-coding genes. Genes Dev. *34*, 132-145. 10.1101/gad.332833.119.
50. Xie, J., Libri, D., and Porrua, O. (2023). Mechanisms of eukaryotic transcription termination at a glance. J. Cell Sci. *136*. 10.1242/jcs.259873.
51. Zeng, Y., Zhang, H.W., Wu, X.X., and Zhang, Y. (2024). Structural basis of exoribonuclease-mediated mRNA transcription termination. Nature *628*, 887-893. 10.1038/s41586-024-07240-3.
52. Benjamin, B., Sanchez, A.M., Garg, A., Schwer, B., and Shuman, S. (2021). Structure-function analysis of fission yeast cleavage and polyadenylation factor (CPF) subunit Ppn1 and its interactions with Dis2 and Swd22. PLoS Genet. *17*, e1009452. 10.1371/journal.pgen.1009452.
53. Collin, P., Jeronimo, C., Poitras, C., and Robert, F. (2019). RNA Polymerase II CTD Tyrosine 1 Is Required for Efficient Termination by the Nrd1-Nab3-Sen1 Pathway. Mol. Cell *73*, 655-669 e657. 10.1016/j.molcel.2018.12.002.
54. Kecman, T., Kus, K., Heo, D.H., Duckett, K., Birot, A., Liberatori, S., Mohammed, S., Geis-Asteggiante, L., Robinson, C.V., and Vasiljeva, L. (2018). Elongation/Termination Factor Exchange Mediated by PP1 Phosphatase Orchestrates Transcription Termination. Cell Rep. *25*, 259-269 e255. 10.1016/j.celrep.2018.09.007.
55. Parua, P.K., Kalan, S., Benjamin, B., Sanso, M., and Fisher, R.P. (2020). Distinct Cdk9-phosphatase switches act at the beginning and end of elongation by RNA polymerase II. Nat. Commun. *11*, 4338. 10.1038/s41467-020-18173-6.
56. Schreieck, A., Easter, A.D., Etzold, S., Wiederhold, K., Lidschreiber, M., Cramer, P., and Passmore, L.A. (2014). RNA polymerase II termination involves C-terminal-domain tyrosine dephosphorylation by CPF subunit Glc7. Nat. Struct. Mol. Biol. *21*, 175-179. 10.1038/nsmb.2753.
57. Fong, N., Brannan, K., Erickson, B., Kim, H., Cortazar, M.A., Sheridan, R.M., Nguyen, T., Karp, S., and Bentley, D.L. (2015). Effects of Transcription Elongation Rate and Xrn2 Exonuclease Activity on RNA Polymerase II Termination Suggest Widespread Kinetic Competition. Mol. Cell *60*, 256-267. 10.1016/j.molcel.2015.09.026.
58. Casanal, A., Kumar, A., Hill, C.H., Easter, A.D., Emsley, P., Degliesposti, G., Gordiyenko, Y., Santhanam, B., Wolf, J., Wiederhold, K., et al. (2017). Architecture of eukaryotic mRNA 3'-end processing machinery. Science *358*, 1056-1059. 10.1126/science.aao6535.
59. Nedea, E., He, X., Kim, M., Pootoolal, J., Zhong, G., Canadien, V., Hughes, T., Buratowski, S., Moore, C.L., and Greenblatt, J. (2003). Organization and function of APT, a subcomplex of the yeast cleavage and polyadenylation factor involved in the formation of mRNA and small nucleolar RNA 3'-ends. J. Biol. Chem. *278*, 33000-33010. 10.1074/jbc.M304454200.

60. Nedea, E., Nalbant, D., Xia, D., Theoharis, N.T., Suter, B., Richardson, C.J., Tatchell, K., Kislinger, T., Greenblatt, J.F., and Nagy, P.L. (2008). The Glc7 phosphatase subunit of the cleavage and polyadenylation factor is essential for transcription termination on snoRNA genes. Mol Cell *29*, 577-587. 10.1016/j.molcel.2007.12.031.
61. Baejen, C., Andreani, J., Torkler, P., Battaglia, S., Schwalb, B., Lidschreiber, M., Maier, K.C., Boltendahl, A., Rus, P., Esslinger, S., et al. (2017). Genome-wide Analysis of RNA Polymerase II Termination at Protein-Coding Genes. Mol. Cell *66*, 38-49 e36. 10.1016/j.molcel.2017.02.009.
62. Kus, K., Carrique, L., Kecman, T., Fournier, M., Hassanein, S.S., Aydin, E., Kilchert, C., Grimes, J.M., and Vasiljeva, L. (2025). DSIF factor Spt5 coordinates transcription, maturation and exoribonucleolysis of RNA polymerase II transcripts. Nat. Commun. *16*, 10. 10.1038/s41467-024-55063-7.
63. Nishimura, K., Fukagawa, T., Takisawa, H., Kakimoto, T., and Kanemaki, M. (2009). An auxin-based degron system for the rapid depletion of proteins in nonplant cells. Nat. Methods *6*, 917-922. 10.1038/nmeth.1401.
64. Miller, C., Schwalb, B., Maier, K., Schulz, D., Dumcke, S., Zacher, B., Mayer, A., Sydow, J., Marcinowski, L., Dolken, L., et al. (2011). Dynamic transcriptome analysis measures rates of mRNA synthesis and decay in yeast. Mol. Syst. Biol. *7*, 458. 10.1038/msb.2010.112.
65. Yesbolatova, A., Saito, Y., Kitamoto, N., Makino-Itou, H., Ajima, R., Nakano, R., Nakaoka, H., Fukui, K., Gamo, K., Tominari, Y., et al. (2020). The auxin-inducible degron 2 technology provides sharp degradation control in yeast, mammalian cells, and mice. Nat. Commun. *11*, 5701. 10.1038/s41467-020-19532-z.
66. An, H., Yang, H., and Lee, D. (2024). Spt5 orchestrates cryptic transcript suppression and transcriptional directionality. Commun. Biol. *7*, 1370. 10.1038/s42003-024-07014-7.
67. Badjatia, N., Rossi, M.J., Bataille, A.R., Mittal, C., Lai, W.K.M., and Pugh, B.F. (2021). Acute stress drives global repression through two independent RNA polymerase II stalling events in *Saccharomyces*. Cell Rep. *34*, 108640. 10.1016/j.celrep.2020.108640.
68. Henriques, T., Scruggs, B.S., Inouye, M.O., Muse, G.W., Williams, L.H., Burkholder, A.B., Lavender, C.A., Fargo, D.C., and Adelman, K. (2018). Widespread transcriptional pausing and elongation control at enhancers. Genes Dev. *32*, 26-41. 10.1101/gad.309351.117.
69. Shetty, A., Kallgren, S.P., Demel, C., Maier, K.C., Spatt, D., Alver, B.H., Cramer, P., Park, P.J., and Winston, F. (2017). Spt5 Plays Vital Roles in the Control of Sense and Antisense Transcription Elongation. Mol. Cell *66*, 77-88 e75. 10.1016/j.molcel.2017.02.023.
70. Aoi, Y., Shah, A.P., Ganesan, S., Soliman, S.H.A., Cho, B.K., Goo, Y.A., Kelleher, N.L., and Shilatifard, A. (2022). SPT6 functions in transcriptional pause/release via PAF1C recruitment. Mol. Cell *82*, 3412-3423 e3415. 10.1016/j.molcel.2022.06.037.
71. Caizzi, L., Monteiro-Martins, S., Schwalb, B., Lysakovskaia, K., Schmitzova, J., Sawicka, A., Chen, Y., Lidschreiber, M., and Cramer, P. (2021). Efficient RNA polymerase II pause release requires U2 snRNP function. Mol. Cell *81*, 1920-1934 e1929. 10.1016/j.molcel.2021.02.016.
72. Fong, N., Kim, H., Zhou, Y., Ji, X., Qiu, J., Saldi, T., Diener, K., Jones, K., Fu, X.D., and Bentley, D.L. (2014). Pre-mRNA splicing is facilitated by an optimal RNA polymerase II elongation rate. Genes Dev. *28*, 2663-2676. 10.1101/gad.252106.114.
73. Maudlin, I.E., and Beggs, J.D. (2019). Spt5 modulates cotranscriptional spliceosome assembly in Saccharomyces cerevisiae. RNA *25*, 1298-1310. 10.1261/rna.070425.119.
74. Connell, Z., Parnell, T.J., McCullough, L.L., Hill, C.P., and Formosa, T. (2022). The interaction between the Spt6-tSH2 domain and Rpb1 affects multiple functions of RNA Polymerase II. Nucleic Acids Res. *50*, 784-802. 10.1093/nar/gkab1262.

75. Narain, A., Bhandare, P., Adhikari, B., Backes, S., Eilers, M., Dolken, L., Schlosser, A., Erhard, F., Baluapuri, A., and Wolf, E. (2021). Targeted protein degradation reveals a direct role of SPT6 in RNAPII elongation and termination. Mol. Cell *81*, 3110-3127 e3114. 10.1016/j.molcel.2021.06.016.
76. Michel, A.H., Hatakeyama, R., Kimmig, P., Arter, M., Peter, M., Matos, J., De Virgilio, C., and Kornmann, B. (2017). Functional mapping of yeast genomes by saturated transposition. Elife *6*. 10.7554/eLife.23570.
77. Michel, A.H., and Kornmann, B. (2022). SAturated Transposon Analysis in Yeast (SATAY) for Deep Functional Mapping of Yeast Genomes. Methods Mol. Biol. *2477*, 349-379. 10.1007/978-1-0716-2257-5_20.
78. Duan, B., Qiu, C., Sze, S.H., and Kaplan, C. (2025). Widespread epistasis shapes RNA Polymerase II active site function and evolution. bioRxiv. 10.1101/2023.02.27.530048.
79. Tang, J., Abovich, N., and Rosbash, M. (1996). Identification and characterization of a yeast gene encoding the U2 small nuclear ribonucleoprotein particle B" protein. Mol. Cell. Biol. *16*, 2787-2795. 10.1128/MCB.16.6.2787.
80. Cui, P., Jin, H., Vutukuru, M.R., and Kaplan, C.D. (2016). Relationships Between RNA Polymerase II Activity and Spt Elongation Factors to Spt- Phenotype and Growth in *Saccharomyces cerevisiae*. G3 (Bethesda) *6*, 2489-2504. 10.1534/g3.116.030346.
81. Hartzog, G.A., Wada, T., Handa, H., and Winston, F. (1998). Evidence that Spt4, Spt5, and Spt6 control transcription elongation by RNA polymerase II in *Saccharomyces cerevisiae*. Genes Dev. *12*, 357-369. 10.1101/gad.12.3.357.
82. Quan, T.K., and Hartzog, G.A. (2010). Histone H3K4 and K36 methylation, Chd1 and Rpd3S oppose the functions of *Saccharomyces cerevisiae* Spt4-Spt5 in transcription. Genetics *184*, 321-334. 10.1534/genetics.109.111526.
83. Cheng, H., He, X., and Moore, C. (2004). The essential WD repeat protein Swd2 has dual functions in RNA polymerase II transcription termination and lysine 4 methylation of histone H3. Mol. Cell. Biol. *24*, 2932-2943. 10.1128/MCB.24.7.2932-2943.2004.
84. Lidschreiber, M., Easter, A.D., Battaglia, S., Rodriguez-Molina, J.B., Casanal, A., Carminati, M., Baejen, C., Grzechnik, P., Maier, K.C., Cramer, P., and Passmore, L.A. (2018). The APT complex is involved in non-coding RNA transcription and is distinct from CPF. Nucleic Acids Res. *46*, 11528-11538. 10.1093/nar/gky845.
85. Russnak, R., Nehrke, K.W., and Platt, T. (1995). *REF2* encodes an RNA-binding protein directly involved in yeast mRNA 3'-end formation. Mol. Cell. Biol. *15*, 1689-1697. 10.1128/MCB.15.3.1689.
86. Francette, A.M., Tripplehorn, S.A., and Arndt, K.M. (2021). The Paf1 Complex: A Keystone of Nuclear Regulation Operating at the Interface of Transcription and Chromatin. J. Mol. Biol. *433*, 166979. 10.1016/j.jmb.2021.166979.
87. Warner, M.H., Roinick, K.L., and Arndt, K.M. (2007). Rtf1 is a multifunctional component of the Paf1 complex that regulates gene expression by directing cotranscriptional histone modification. Mol. Cell. Biol. *27*, 6103-6115. 10.1128/MCB.00772-07.
88. Carminati, M., Rodriguez-Molina, J.B., Manav, M.C., Bellini, D., and Passmore, L.A. (2023). A direct interaction between CPF and RNA Pol II links RNA 3' end processing to transcription. Mol. Cell *83*, 4461-4478 e4413. 10.1016/j.molcel.2023.11.004.
89. Wang, Y., Ding, Z., Liu, X., Bao, Y., Huang, M., Wong, C.C.L., Hong, X., and Cong, Y. (2018). Architecture and subunit arrangement of the complete *Saccharomyces cerevisiae* COMPASS complex. Sci. Rep. *8*, 17405. 10.1038/s41598-018-35609-8.
90. Haruki, H., Nishikawa, J., and Laemmli, U.K. (2008). The anchor-away technique: rapid, conditional establishment of yeast mutant phenotypes. Mol. Cell *31*, 925-932. 10.1016/j.molcel.2008.07.020.

91. Tu, J., and Carlson, M. (1994). The GLC7 type 1 protein phosphatase is required for glucose repression in *Saccharomyces cerevisiae*. Mol. Cell. Biol. *14*, 6789-6796. 10.1128/mcb.14.10.6789-6796.1994.
92. Nordick, K., Hoffman, M.G., Betz, J.L., and Jaehning, J.A. (2008). Direct interactions between the Paf1 complex and a cleavage and polyadenylation factor are revealed by dissociation of Paf1 from RNA polymerase II. Eukaryot. Cell *7*, 1158-1167. 10.1128/EC.00434-07.
93. Santana, J.F., Spector, B.M., Suarez, G.A., Luse, D.S., and Price, D.H. (2024). NELF focuses sites of initiation and maintains promoter architecture. Nucleic Acids Res. *52*, 2977-2994. 10.1093/nar/gkad1253.
94. Malik, I., Qiu, C., Snavely, T., and Kaplan, C.D. (2017). Wide-ranging and unexpected consequences of altered Pol II catalytic activity in vivo. Nucleic Acids Res. *45*, 4431-4451. 10.1093/nar/gkx037.
95. Ehara, H., Yokoyama, T., Shigematsu, H., Yokoyama, S., Shirouzu, M., and Sekine, S.I. (2017). Structure of the complete elongation complex of RNA polymerase II with basal factors. Science *357*, 921-924. 10.1126/science.aan8552.
96. Sdano, M.A., Fulcher, J.M., Palani, S., Chandrasekharan, M.B., Parnell, T.J., Whitby, F.G., Formosa, T., and Hill, C.P. (2017). A novel SH2 recognition mechanism recruits Spt6 to the doubly phosphorylated RNA polymerase II linker at sites of transcription. Elife *6*. 10.7554/eLife.28723.
97. Farnung, L., Ochmann, M., Engeholm, M., and Cramer, P. (2021). Structural basis of nucleosome transcription mediated by Chd1 and FACT. Nat. Struct. Mol. Biol. *28*, 382-387. 10.1038/s41594-021-00578-6.
98. Miller, C.L.W., Warner, J.L., and Winston, F. (2023). Insights into Spt6: a histone chaperone that functions in transcription, DNA replication, and genome stability. Trends Genet. *39*, 858-872. 10.1016/j.tig.2023.06.008.
99. Braberg, H., Jin, H., Moehle, E.A., Chan, Y.A., Wang, S., Shales, M., Benschop, J.J., Morris, J.H., Qiu, C., Hu, F., et al. (2013). From structure to systems: high-resolution, quantitative genetic analysis of RNA polymerase II. Cell *154*, 775-788. 10.1016/j.cell.2013.07.033.
100. Jin, H., and Kaplan, C.D. (2014). Relationships of RNA polymerase II genetic interactors to transcription start site usage defects and growth in *Saccharomyces cerevisiae*. G3 (Bethesda) *5*, 21-33. 10.1534/g3.114.015180.
101. Mimoso, C.A., and Adelman, K. (2023). U1 snRNP increases RNA Pol II elongation rate to enable synthesis of long genes. Mol. Cell *83*, 1264-1279 e1210. 10.1016/j.molcel.2023.03.002.
102. Shenasa, H., and Bentley, D.L. (2023). Pre-mRNA splicing and its cotranscriptional connections. Trends Genet. *39*, 672-685. 10.1016/j.tig.2023.04.008.
103. Hossain, M.A., Claggett, J.M., Nguyen, T., and Johnson, T.L. (2009). The cap binding complex influences H2B ubiquitination by facilitating splicing of the SUS1 pre-mRNA. RNA *15*, 1515-1527. 10.1261/rna.1540409.
104. Hossain, M.A., Rodriguez, C.M., and Johnson, T.L. (2011). Key features of the two-intron *Saccharomyces cerevisiae* gene *SUS1* contribute to its alternative splicing. Nucleic Acids Res. *39*, 8612-8627. 10.1093/nar/gkr497.
105. Shieh, G.S., Pan, C.H., Wu, J.H., Sun, Y.J., Wang, C.C., Hsiao, W.C., Lin, C.Y., Tung, L., Chang, T.H., Fleming, A.B., et al. (2011). H2B ubiquitylation is part of chromatin architecture that marks exon-intron structure in budding yeast. BMC Genomics *12*, 627. 10.1186/1471-2164-12-627.
106. Erickson, B., Fedoryshchak, R., Fong, N., Sheridan, R., Larson, K.Y., Saviola, A.J., Mouilleron, S., Hansen, K.C., Treisman, R., and Bentley, D.L. (2025). PP1/PNUTS

phosphatase binds the restrictor complex and stimulates RNA Pol II transcription termination. Cell Rep. *44*, 115564. 10.1016/j.celrep.2025.115564.
107. Ellison, M.A., Lederer, A.R., Warner, M.H., Mavrich, T.N., Raupach, E.A., Heisler, L.E., Nislow, C., Lee, M.T., and Arndt, K.M. (2019). The Paf1 Complex Broadly Impacts the Transcriptome of *Saccharomyces cerevisiae*. Genetics *212*, 711-728. 10.1534/genetics.119.302262.
108. Sheldon, K.E., Mauger, D.M., and Arndt, K.M. (2005). A Requirement for the *Saccharomyces cerevisiae* Paf1 complex in snoRNA 3' end formation. Mol. Cell *20*, 225-236. 10.1016/j.molcel.2005.08.026.
109. Terzi, N., Churchman, L.S., Vasiljeva, L., Weissman, J., and Buratowski, S. (2011). H3K4 trimethylation by Set1 promotes efficient termination by the Nrd1-Nab3-Sen1 pathway. Mol. Cell. Biol. *31*, 3569-3583. 10.1128/MCB.05590-11.
110. Tomson, B.N., Crisucci, E.M., Heisler, L.E., Gebbia, M., Nislow, C., and Arndt, K.M. (2013). Effects of the Paf1 complex and histone modifications on snoRNA 3'-end formation reveal broad and locus-specific regulation. Mol. Cell. Biol. *33*, 170-182. 10.1128/MCB.01233-12.
111. Tomson, B.N., Davis, C.P., Warner, M.H., and Arndt, K.M. (2011). Identification of a role for histone H2B ubiquitylation in noncoding RNA 3'-end formation through mutational analysis of Rtf1 in *Saccharomyces cerevisiae*. Genetics *188*, 273-289. 10.1534/genetics.111.128645.
112. Geisberg, J.V., Moqtaderi, Z., and Struhl, K. (2020). The transcriptional elongation rate regulates alternative polyadenylation in yeast. Elife *9*. 10.7554/eLife.59810.
113. Yang, Y., Li, W., Hoque, M., Hou, L., Shen, S., Tian, B., and Dynlacht, B.D. (2016). PAF Complex Plays Novel Subunit-Specific Roles in Alternative Cleavage and Polyadenylation. PLoS Genet. *12*, e1005794. 10.1371/journal.pgen.1005794.
114. Ahn, S.H., Kim, M., and Buratowski, S. (2004). Phosphorylation of serine 2 within the RNA polymerase II C-terminal domain couples transcription and 3' end processing. Mol. Cell *13*, 67-76. 10.1016/s1097-2765(03)00492-1.
115. Lunde, B.M., Reichow, S.L., Kim, M., Suh, H., Leeper, T.C., Yang, F., Mutschler, H., Buratowski, S., Meinhart, A., and Varani, G. (2010). Cooperative interaction of transcription termination factors with the RNA polymerase II C-terminal domain. Nat. Struct. Mol. Biol. *17*, 1195-1201. 10.1038/nsmb.1893.
116. Meinhart, A., and Cramer, P. (2004). Recognition of RNA polymerase II carboxy-terminal domain by 3'-RNA-processing factors. Nature *430*, 223-226. 10.1038/nature02679.
117. Mayer, A., Heidemann, M., Lidschreiber, M., Schreieck, A., Sun, M., Hintermair, C., Kremmer, E., Eick, D., and Cramer, P. (2012). CTD tyrosine phosphorylation impairs termination factor recruitment to RNA polymerase II. Science *336*, 1723-1725. 10.1126/science.1219651.
118. Reim, N.I., Chuang, J., Jain, D., Alver, B.H., Park, P.J., and Winston, F. (2020). The conserved elongation factor Spn1 is required for normal transcription, histone modifications, and splicing in *Saccharomyces cerevisiae*. Nucleic Acids Res. *48*, 10241-10258. 10.1093/nar/gkaa745.
119. Meyer, P.A., Li, S., Zhang, M., Yamada, K., Takagi, Y., Hartzog, G.A., and Fu, J. (2015). Structures and Functions of the Multiple KOW Domains of Transcription Elongation Factor Spt5. Mol. Cell. Biol. *35*, 3354-3369. 10.1128/MCB.00520-15.
120. Gene Ontology, C., Aleksander, S.A., Balhoff, J., Carbon, S., Cherry, J.M., Drabkin, H.J., Ebert, D., Feuermann, M., Gaudet, P., Harris, N.L., et al. (2023). The Gene Ontology knowledgebase in 2023. Genetics *224*. 10.1093/genetics/iyad031.
121. McCullough, L., Connell, Z., Petersen, C., and Formosa, T. (2015). The Abundant Histone Chaperones Spt6 and FACT Collaborate to Assemble, Inspect, and Maintain

Chromatin Structure in *Saccharomyces cerevisiae*. Genetics *201*, 1031-1045. 10.1534/genetics.115.180794.
122. Tanaka, S., Miyazawa-Onami, M., Iida, T., and Araki, H. (2015). iAID: an improved auxin-inducible degron system for the construction of a 'tight' conditional mutant in the budding yeast *Saccharomyces cerevisiae*. Yeast *32*, 567-581. 10.1002/yea.3080.
123. Van Driessche, B., Tafforeau, L., Hentges, P., Carr, A.M., and Vandenhaute, J. (2005). Additional vectors for PCR-based gene tagging in *Saccharomyces cerevisiae* and *Schizosaccharomyces pombe* using nourseothricin resistance. Yeast *22*, 1061-1068. 10.1002/yea.1293.
124. Longtine, M.S., McKenzie, A., 3rd, Demarini, D.J., Shah, N.G., Wach, A., Brachat, A., Philippsen, P., and Pringle, J.R. (1998). Additional modules for versatile and economical PCR-based gene deletion and modification in *Saccharomyces cerevisiae*. Yeast *14*, 953-961. 10.1002/(SICI)1097-0061(199807)14:10<953::AID-YEA293>3.0.CO;2-U.
125. Laughery, M.F., Hunter, T., Brown, A., Hoopes, J., Ostbye, T., Shumaker, T., and Wyrick, J.J. (2015). New vectors for simple and streamlined CRISPR-Cas9 genome editing in *Saccharomyces cerevisiae*. Yeast *32*, 711-720. 10.1002/yea.3098.
126. Langmead, B., and Salzberg, S.L. (2012). Fast gapped-read alignment with Bowtie 2. Nat. Methods *9*, 357-359. 10.1038/nmeth.1923.
127. Li, H., Handsaker, B., Wysoker, A., Fennell, T., Ruan, J., Homer, N., Marth, G., Abecasis, G., Durbin, R., and Genome Project Data Processing, S. (2009). The Sequence Alignment/Map format and SAMtools. Bioinformatics *25*, 2078-2079. 10.1093/bioinformatics/btp352.
128. Barnett, D.W., Garrison, E.K., Quinlan, A.R., Stromberg, M.P., and Marth, G.T. (2011). BamTools: a C++ API and toolkit for analyzing and managing BAM files. Bioinformatics *27*, 1691-1692. 10.1093/bioinformatics/btr174.
129. Quinlan, A.R., and Hall, I.M. (2010). BEDTools: a flexible suite of utilities for comparing genomic features. Bioinformatics *26*, 841-842. 10.1093/bioinformatics/btq033.
130. Ramirez, F., Ryan, D.P., Gruning, B., Bhardwaj, V., Kilpert, F., Richter, A.S., Heyne, S., Dundar, F., and Manke, T. (2016). deepTools2: a next generation web server for deep-sequencing data analysis. Nucleic Acids Res. *44*, W160-165. 10.1093/nar/gkw257.
131. Tarasov, A., Vilella, A.J., Cuppen, E., Nijman, I.J., and Prins, P. (2015). Sambamba: fast processing of NGS alignment formats. Bioinformatics *31*, 2032-2034. 10.1093/bioinformatics/btv098.
132. Tange, O. (2011). GNU parallel - the command-line power tool. . The Usenix Magazine *36*, 42-47. 10.5281/zenodo.16303.
133. Kim, D., Paggi, J.M., Park, C., Bennett, C., and Salzberg, S.L. (2019). Graph-based genome alignment and genotyping with HISAT2 and HISAT-genotype. Nat. Biotechnol. *37*, 907-915. 10.1038/s41587-019-0201-4.
134. Love, M.I., Huber, W., and Anders, S. (2014). Moderated estimation of fold change and dispersion for RNA-seq data with DESeq2. Genome Biol. *15*, 550. 10.1186/s13059-014-0550-8.
135. Yu, G., Wang, L.G., Han, Y., and He, Q.Y. (2012). clusterProfiler: an R package for comparing biological themes among gene clusters. OMICS *16*, 284-287. 10.1089/omi.2011.0118.
136. Liao, Y., Smyth, G.K., and Shi, W. (2014). featureCounts: an efficient general purpose program for assigning sequence reads to genomic features. Bioinformatics *30*, 923-930. 10.1093/bioinformatics/btt656.
137. Chen, S. (2023). Ultrafast one-pass FASTQ data preprocessing, quality control, and deduplication using fastp. Imeta *2*, e107. 10.1002/imt2.107.

138. Pau, G., Fuchs, F., Sklyar, O., Boutros, M., and Huber, W. (2010). EBImage--an R package for image processing with applications to cellular phenotypes. Bioinformatics *26*, 979-981. 10.1093/bioinformatics/btq046.
139. Wickham, H. (2011). ggplot2. Wiley Interdis. Rev. Comput. Stat. *3*, 180-185. 10.1002/wics.147.
140. Perez, G., Barber, G.P., Benet-Pages, A., Casper, J., Clawson, H., Diekhans, M., Fischer, C., Gonzalez, J.N., Hinrichs, A.S., Lee, C.M., et al. (2025). The UCSC Genome Browser database: 2025 update. Nucleic Acids Res. *53*, D1243-D1249. 10.1093/nar/gkae974.
141. Robinson, J.T., Thorvaldsdottir, H., Winckler, W., Guttman, M., Lander, E.S., Getz, G., and Mesirov, J.P. (2011). Integrative genomics viewer. Nat. Biotechnol. *29*, 24-26. 10.1038/nbt.1754.
142. Winston, F., Dollard, C., and Ricupero-Hovasse, S.L. (1995). Construction of a set of convenient Saccharomyces cerevisiae strains that are isogenic to S288C. Yeast *11*, 53-55. 10.1002/yea.320110107.
143. Rose, M.D., Winston, F., and Hieter, P. (1990). Methods in Yeast Genetics: A Laboratory Course Manual (Cold Spring Harbor Laboratory Press, Cold Spring Harbor, NY).
144. Alexander, R.D., Barrass, J.D., Dichtl, B., Kos, M., Obtulowicz, T., Robert, M.C., Koper, M., Karkusiewicz, I., Mariconti, L., Tollervey, D., et al. (2010). RiboSys, a high-resolution, quantitative approach to measure the *in vivo* kinetics of pre-mRNA splicing and 3'-end processing in *Saccharomyces cerevisiae*. RNA *16*, 2570-2580. 10.1261/rna.2162610.
145. Kushnirov, V.V. (2000). Rapid and reliable protein extraction from yeast. Yeast *16*, 857-860. 10.1002/1097-0061(20000630)16:9<857::AID-YEA561>3.0.CO;2-B.
146. Jeronimo, C., Poitras, C., and Robert, F. (2019). Histone Recycling by FACT and Spt6 during Transcription Prevents the Scrambling of Histone Modifications. Cell Rep. *28*, 1206-1218 e1208. 10.1016/j.celrep.2019.06.097.
147. Barrass, J.D., and Beggs, J.D. (2019). Extremely Rapid and Specific Metabolic Labelling of RNA In Vivo with 4-Thiouracil (Ers4tU). J. Vis. Exp. 10.3791/59952.
148. Prevorovsky, M., Halova, M., Abrhamova, K., Libus, J., and Folk, P. (2016). Workflow for Genome-Wide Determination of Pre-mRNA Splicing Efficiency from Yeast RNA-seq Data. Biomed. Res. Int. *2016*, 4783841. 10.1155/2016/4783841.
149. Wong, E.D., Miyasato, S.R., Aleksander, S., Karra, K., Nash, R.S., Skrzypek, M.S., Weng, S., Engel, S.R., and Cherry, J.M. (2023). *Saccharomyces* genome database update: server architecture, pan-genome nomenclature, and external resources. Genetics *224*. 10.1093/genetics/iyac191.

Figure 1

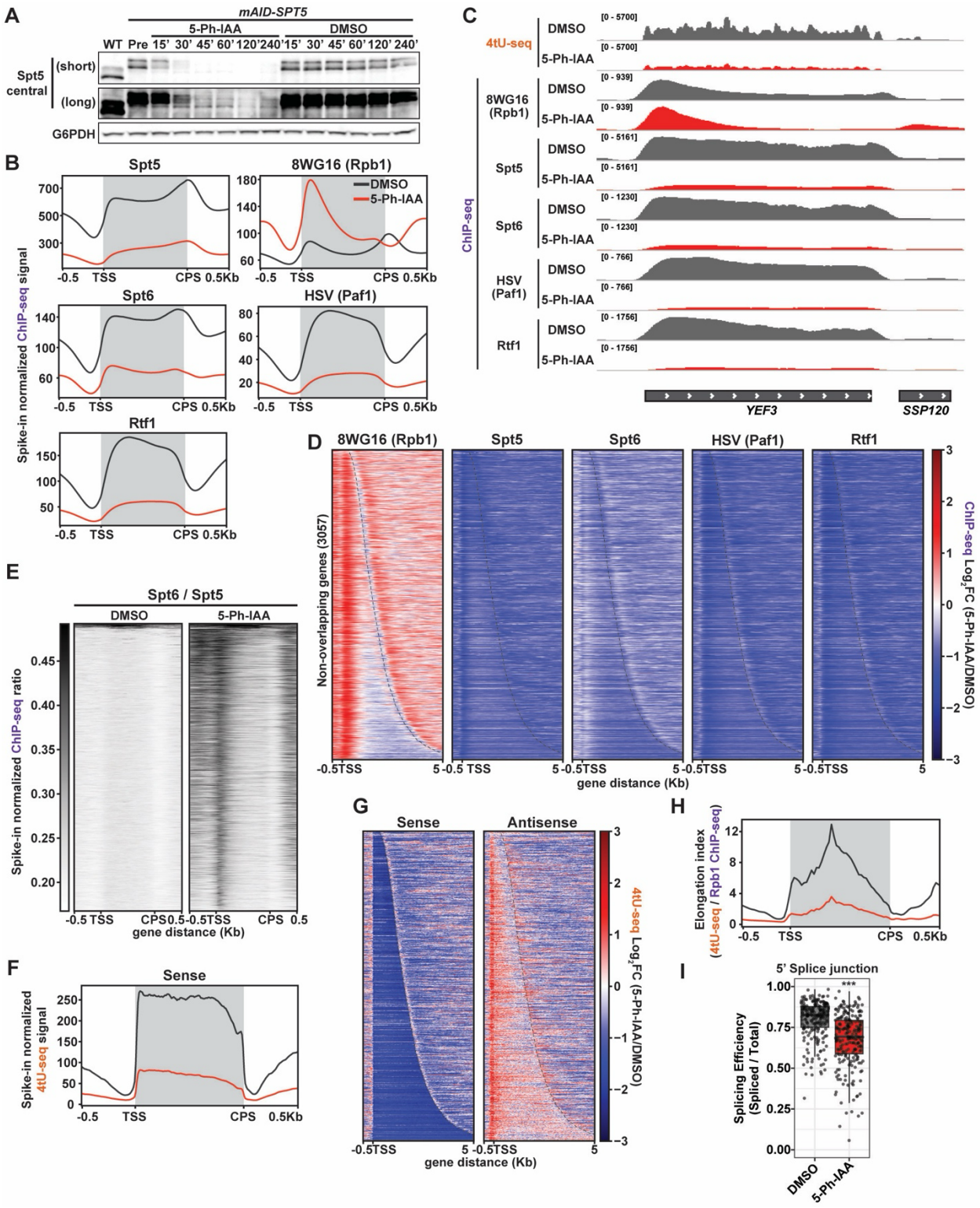
A
mAID-SPT5
5-Ph-IAA
DMSO
WT Pre 15' 30' 45' 60' 120' 240' 15' 30' 45' 60' 120' 240'
Spt5 central
(short)
(long)
G6PDH
B
Spt5
8WG16 (Rpb1)
DMSO
5-Ph-IAA
Spt6
HSV (Paf1)
Rtf1
Spike-in normalized ChIP-seq signal
-0.5 TSS CPS 0.5Kb
C
4tU-seq
ChIP-seq
8WG16 (Rpb1)
Spt5
Spt6
HSV (Paf1)
Rtf1
YEF3
SSP120
D
8WG16 (Rpb1)
Spt5
Spt6
HSV (Paf1)
Rtf1
Non-overlapping genes (3057)
gene distance (Kb)
ChIP-seq Log2FC (5-Ph-IAA/DMSO)
E
Spt6 / Spt5
DMSO
5-Ph-IAA
Spike-in normalized ChIP-seq ratio
gene distance (Kb)
F
Sense
Spike-in normalized 4tU-seq signal
G
Sense
Antisense
4tU-seq Log2FC (5-Ph-IAA/DMSO)
gene distance (Kb)
H
Elongation index (4tU-seq / Rpb1 ChIP-seq)
I
5' Splice junction
Splicing Efficiency (Spliced / Total)
DMSO
5-Ph-IAA

Figure 2

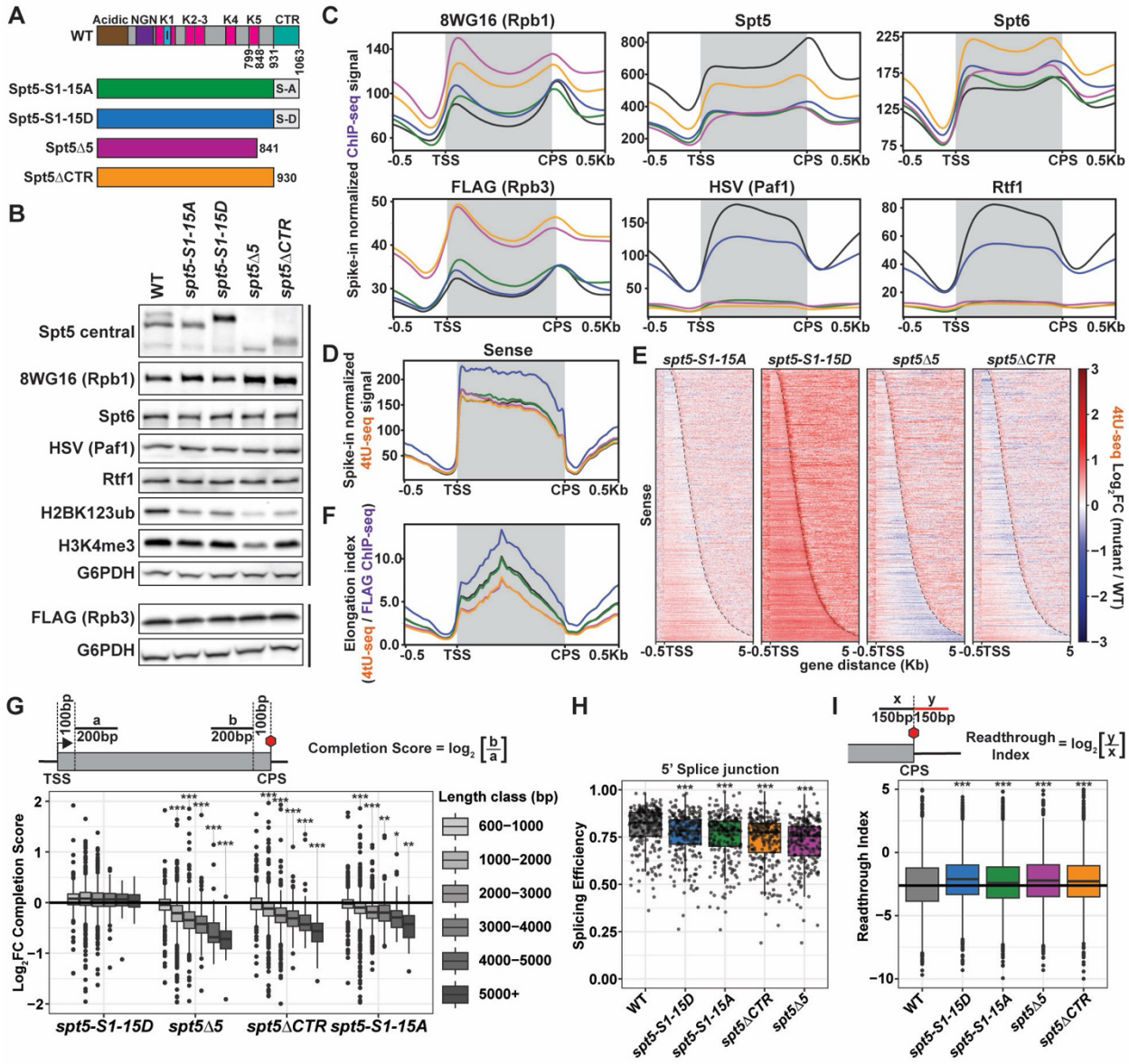
A
Acidic NGN K1 K2-3 K4 K5 CTR
WT
799 848 931 1063
Spt5-S1-15A
S-A
Spt5-S1-15D
S-D
Spt5Δ5
841
Spt5ΔCTR
930
B
WT
spt5-S1-15A
spt5-S1-15D
spt5Δ5
spt5ΔCTR
Spt5 central
8WG16 (Rpb1)
Spt6
HSV (Paf1)
Rtf1
H2BK123ub
H3K4me3
G6PDH
FLAG (Rpb3)
G6PDH
C
8WG16 (Rpb1)
Spt5
Spt6
FLAG (Rpb3)
HSV (Paf1)
Rtf1
Spike-in normalized ChIP-seq signal
-0.5 TSS CPS 0.5Kb
D
Sense
Spike-in normalized 4tU-seq signal
E
spt5-S1-15A
spt5-S1-15D
spt5Δ5
spt5ΔCTR
Sense
gene distance (Kb)
4tU-seq Log2FC (mutant / WT)
F
Elongation index (4tU-seq / FLAG ChIP-seq)
G
100bp
a
200bp
b
200bp
100bp
TSS
CPS
Completion Score = log2 [b/a]
Log2FC Completion Score
Length class (bp)
600−1000
1000−2000
2000−3000
3000−4000
4000−5000
5000+
spt5-S1-15D
spt5Δ5
spt5ΔCTR
spt5-S1-15A
H
5' Splice junction
Splicing Efficiency
WT
spt5-S1-15D
spt5-S1-15A
spt5ΔCTR
spt5Δ5
I
x
y
150bp
150bp
CPS
Readthrough Index = log2 [y/x]
Readthrough Index
WT
spt5-S1-15D
spt5-S1-15A
spt5Δ5
spt5ΔCTR

Figure 3

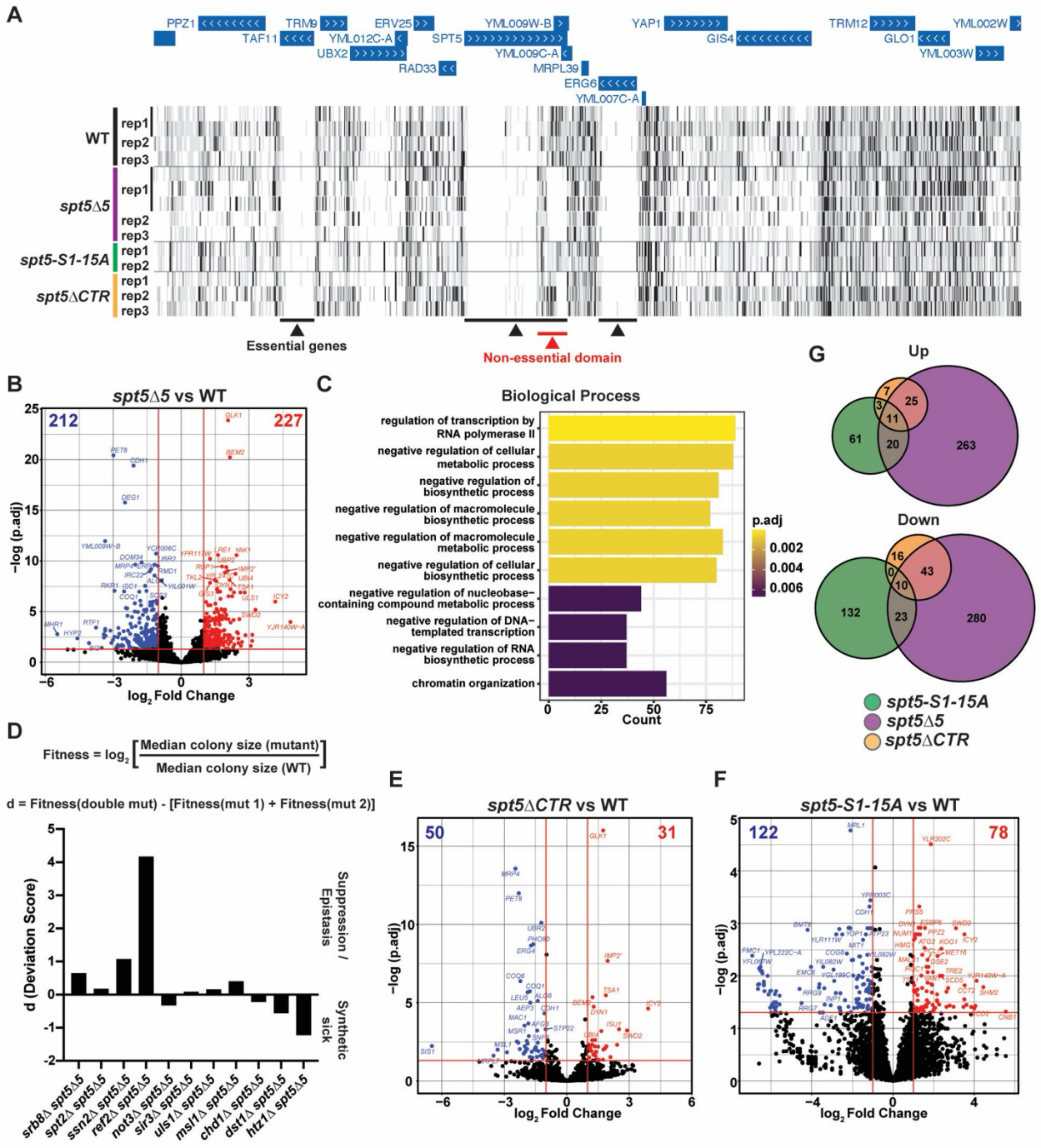
A
PPZ1
TAF11
TRM9
YML012C-A
UBX2
ERV25
RAD33
YML009W-B
SPT5
YML009C-A
MRPL39
ERG6
YML007C-A
YAP1
GIS4
TRM12
GLO1
YML002W
YML003W
WT
rep1
rep2
rep3
spt5Δ5
spt5-S1-15A
spt5ΔCTR
Essential genes
Non-essential domain
B
spt5Δ5 vs WT
212
227
−log (p.adj)
log2 Fold Change
C
Biological Process
regulation of transcription by RNA polymerase II
negative regulation of cellular metabolic process
negative regulation of biosynthetic process
negative regulation of macromolecule biosynthetic process
negative regulation of macromolecule metabolic process
negative regulation of cellular biosynthetic process
negative regulation of nucleobase−containing compound metabolic process
negative regulation of DNA−templated transcription
negative regulation of RNA biosynthetic process
chromatin organization
p.adj
0.002
0.004
0.006
Count
G
Up
61
7
3
25
11
20
263
Down
16
0
43
10
132
23
280
spt5-S1-15A
spt5Δ5
spt5ΔCTR
D
Fitness = log2 [Median colony size (mutant) / Median colony size (WT)]
d = Fitness(double mut) - [Fitness(mut 1) + Fitness(mut 2)]
d (Deviation Score)
Suppression / Epistasis
Synthetic sick
srb8Δ spt5Δ5
spt2Δ spt5Δ5
ssn2Δ spt5Δ5
ref2Δ spt5Δ5
not3Δ spt5Δ5
sir3Δ spt5Δ5
uls1Δ spt5Δ5
msl1Δ spt5Δ5
chd1Δ spt5Δ5
dst1Δ spt5Δ5
htz1Δ spt5Δ5
E
spt5ΔCTR vs WT
50
31
−log (p.adj)
log2 Fold Change
F
spt5-S1-15A vs WT
122
78
−log (p.adj)
log2 Fold Change

Figure 4

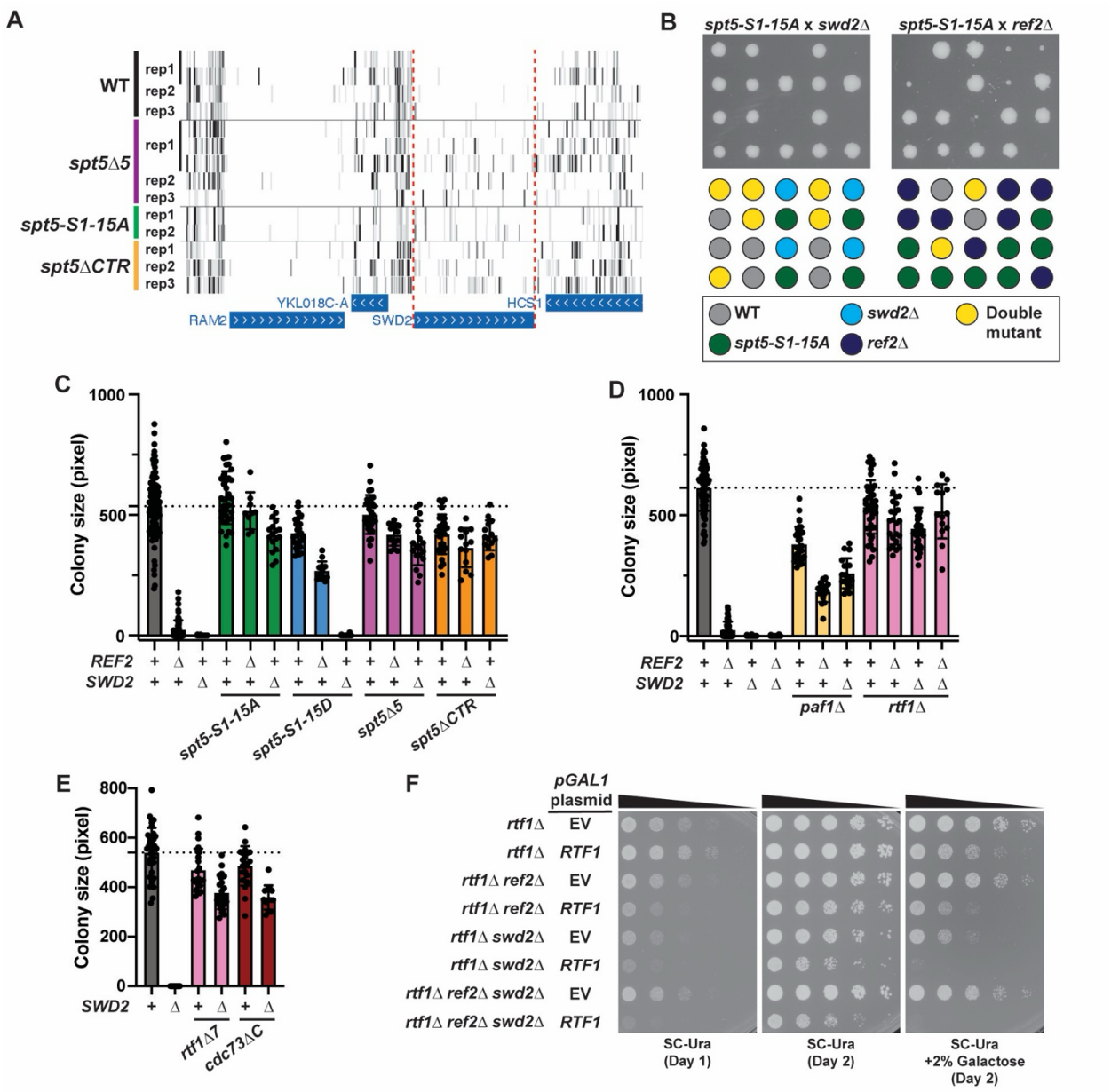
A
WT
rep1
rep2
rep3
spt5Δ5
rep1
rep2
rep3
spt5-S1-15A
rep1
rep2
spt5ΔCTR
rep1
rep2
rep3
YKL018C-A
HCS1
RAM2
SWD2
B
spt5-S1-15A x swd2Δ
spt5-S1-15A x ref2Δ
WT
swd2Δ
Double mutant
spt5-S1-15A
ref2Δ
C
Colony size (pixel)
1000
500
0
REF2
SWD2
spt5-S1-15A
spt5-S1-15D
spt5Δ5
spt5ΔCTR
D
Colony size (pixel)
1000
500
0
REF2
SWD2
paf1Δ
rtf1Δ
E
Colony size (pixel)
800
600
400
200
0
SWD2
rtf1Δ7
cdc73ΔC
F
pGAL1 plasmid
rtf1Δ EV
rtf1Δ RTF1
rtf1Δ ref2Δ EV
rtf1Δ ref2Δ RTF1
rtf1Δ swd2Δ EV
rtf1Δ swd2Δ RTF1
rtf1Δ ref2Δ swd2Δ EV
rtf1Δ ref2Δ swd2Δ RTF1
SC-Ura (Day 1)
SC-Ura (Day 2)
SC-Ura +2% Galactose (Day 2)

Figure 5

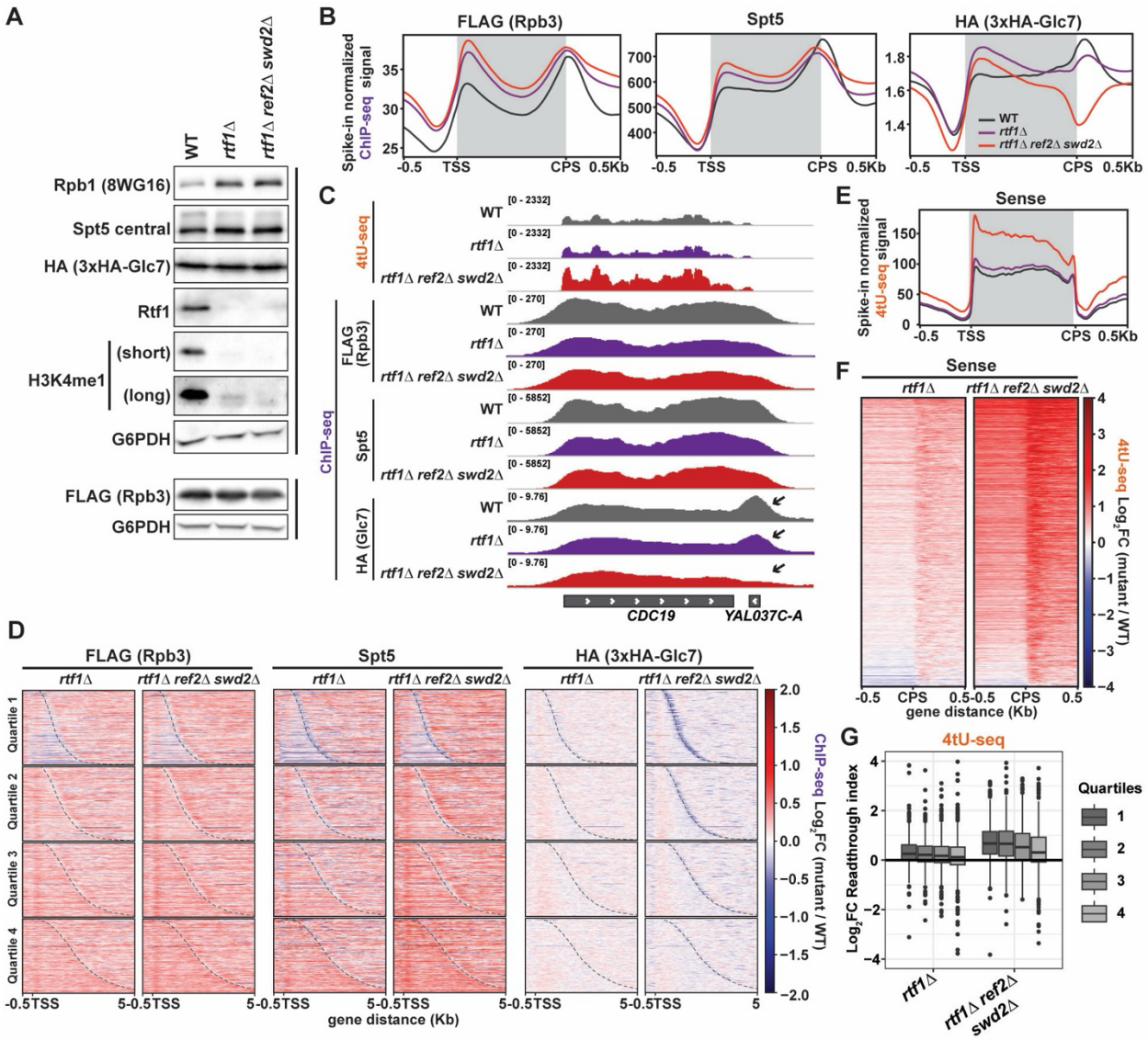
A
WT
rtf1Δ
rtf1Δ ref2Δ swd2Δ
Rpb1 (8WG16)
Spt5 central
HA (3xHA-Glc7)
Rtf1
H3K4me1
(short)
(long)
G6PDH
FLAG (Rpb3)
G6PDH
B
FLAG (Rpb3)
Spt5
HA (3xHA-Glc7)
Spike-in normalized ChIP-seq signal
-0.5 TSS CPS 0.5Kb
C
4tU-seq
ChIP-seq
FLAG (Rpb3)
Spt5
HA (Glc7)
CDC19
YAL037C-A
D
FLAG (Rpb3)
Spt5
HA (3xHA-Glc7)
Quartile 1
Quartile 2
Quartile 3
Quartile 4
ChIP-seq Log2FC (mutant / WT)
gene distance (Kb)
E
Sense
Spike-in normalized 4tU-seq signal
F
Sense
4tU-seq Log2FC (mutant / WT)
gene distance (Kb)
G
4tU-seq
Log2FC Readthrough index
Quartiles
rtf1Δ
rtf1Δ ref2Δ swd2Δ

Figure 6

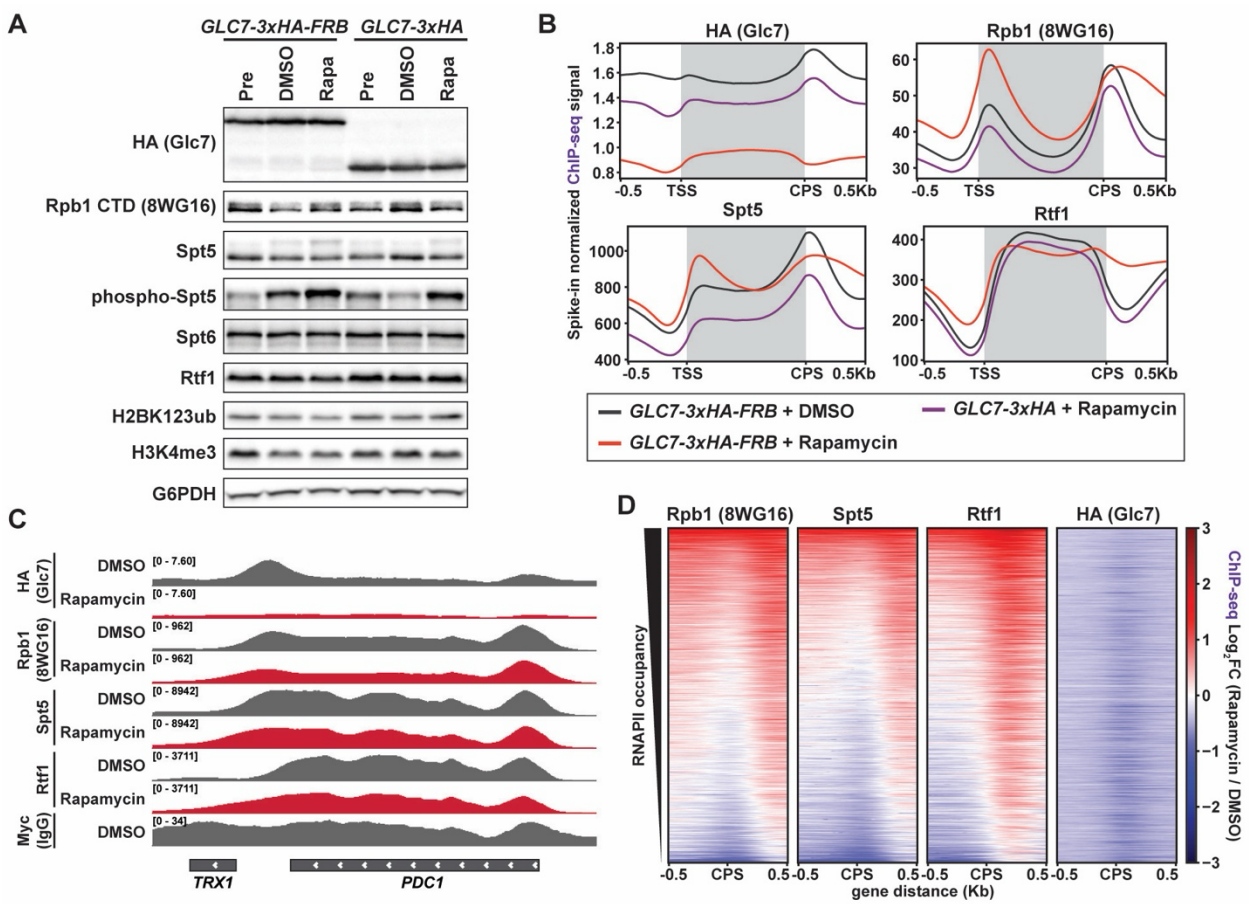
A
GLC7-3xHA-FRB
GLC7-3xHA
Pre
DMSO
Rapa
Pre
DMSO
Rapa
HA (Glc7)
Rpb1 CTD (8WG16)
Spt5
phospho-Spt5
Spt6
Rtf1
H2BK123ub
H3K4me3
G6PDH
B
HA (Glc7)
Rpb1 (8WG16)
Spt5
Rtf1
Spike-in normalized ChIP-seq signal
-0.5
TSS
CPS
0.5Kb
GLC7-3xHA-FRB + DMSO
GLC7-3xHA-FRB + Rapamycin
GLC7-3xHA + Rapamycin
C
HA (Glc7)
Rpb1 (8WG16)
Spt5
Rtf1
Myc (IgG)
DMSO
Rapamycin
[0 - 7.60]
[0 - 962]
[0 - 8942]
[0 - 3711]
[0 - 34]
TRX1
PDC1
D
Rpb1 (8WG16)
Spt5
Rtf1
HA (Glc7)
RNAPII occupancy
-0.5
CPS
0.5
gene distance (Kb)
ChIP-seq Log2FC (Rapamycin / DMSO)

Figure 7

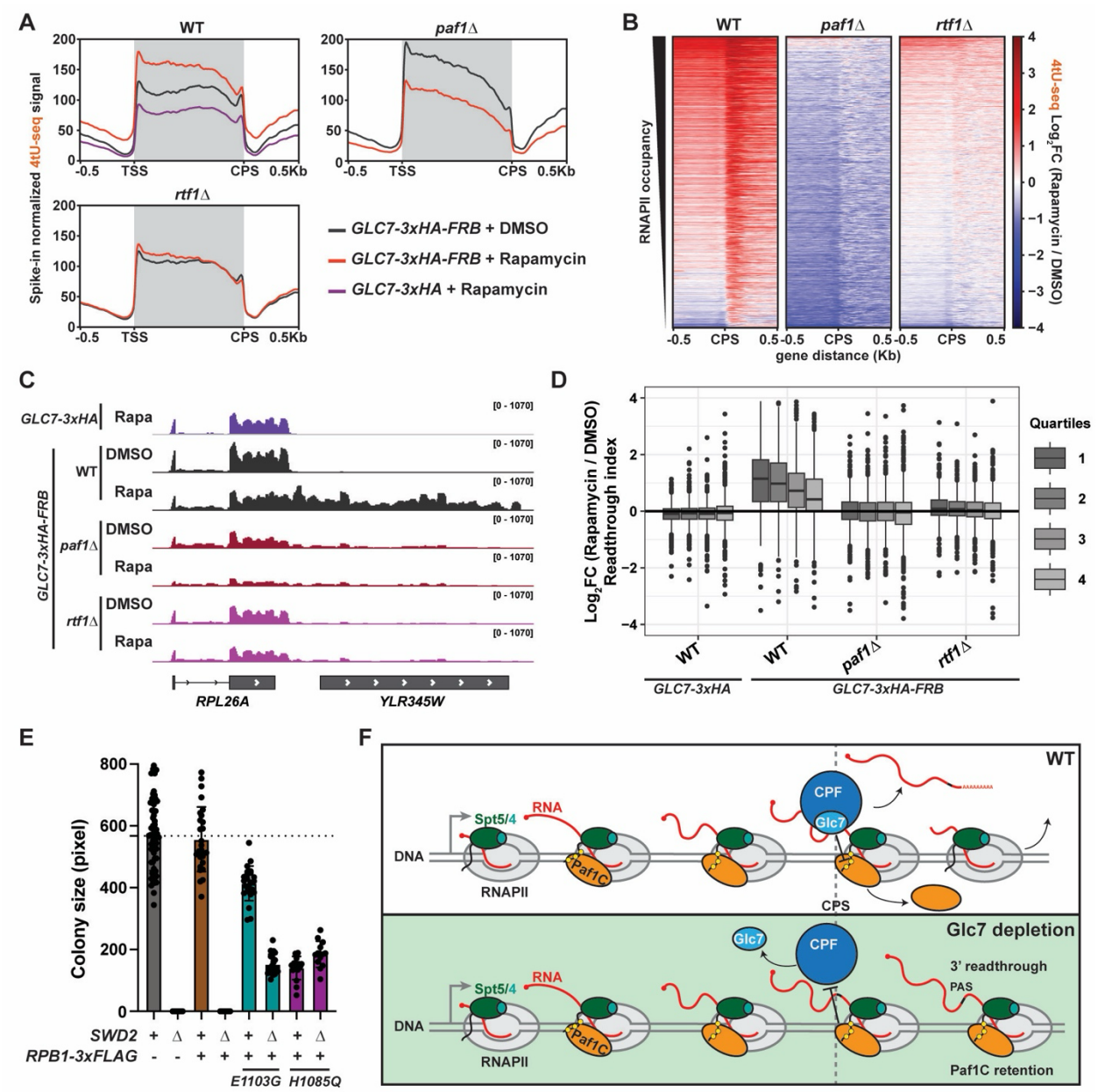
A
WT
paf1Δ
rtf1Δ
Spike-in normalized 4tU-seq signal
-0.5 TSS CPS 0.5Kb
GLC7-3xHA-FRB + DMSO
GLC7-3xHA-FRB + Rapamycin
GLC7-3xHA + Rapamycin
B
RNAPII occupancy
gene distance (Kb)
4tU-seq Log2FC (Rapamycin / DMSO)
C
GLC7-3xHA
GLC7-3xHA-FRB
Rapa
DMSO
[0 - 1070]
RPL26A
YLR345W
D
Log2FC (Rapamycin / DMSO) Readthrough index
Quartiles
GLC7-3xHA
GLC7-3xHA-FRB
E
Colony size (pixel)
SWD2
RPB1-3xFLAG
E1103G
H1085Q
F
WT
Glc7 depletion
DNA
RNAPII
Spt5/4
RNA
Paf1C
CPF
Glc7
CPS
3' readthrough
PAS
Paf1C retention